

國立交通大學
材料科學與工程學研究所
碩士論文

新式含接枝型聚苯乙烯起孔劑之甲基
矽氧烷低介電材料製成及結構特性分析

**Novel Porous Low-k Materials MSQ by
Grafting PS-Siloxane porogen: Synthesis,
Structure, and Pore Morphology**



研究生：邱詩雅

指導教授：呂志鵬 博士

中華民國九十八年七月

新式含接枝型聚苯乙烯起孔劑之甲基矽氧烷低介電材料製成及結構特性分析

Novel Porous Low-k MSQ by Grafting PS-Siloxane porogen: Synthesis, Pore Morphology and Properties

研 究 生：邱詩雅

Student : Shih-ya Chiu

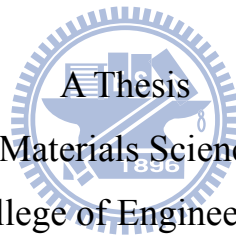
指導教授：呂志鵬 教授

Advisor : Dr. Jihperng Leu

國立交通大學

材料科學與工程學系

碩士論文



Submitted to Department of Materials Science and Engineering

College of Engineering

National Chiao Tung University

in Partial Fulfillment of the Requirements

for the Degree of

Master

in

Materials Science and Engineering

July 2009

Hsinchu, Taiwan, Republic of China

新式含接枝型聚苯乙烯起孔洞劑之甲基矽氧烷低介電材料製成及結構特性分析

新式甲基矽氧烷接枝聚苯乙烯低介電材料製成及結構特性分析

研究生：邱詩雅

指導教授：呂志鵬 博士

國立交通大學材料科學與工程學系碩士班

摘 要

本研究以 Solid-First™ 方法製備多孔性低介電薄膜：以旋塗性質良好的甲基矽氧烷（MSQ，methylsilsesquioxane）為基材，並以原子轉移自由基聚合反應（ATRP）合成的含有矽氧烷的聚苯乙烯（PS-siloxane）作為高溫起孔洞劑（porogen），並以接枝（Graft）方式將兩者結合在一起，即：甲基矽氧烷接枝聚苯乙烯。而起孔洞劑在金屬層完成後才會被燒除，解決了初成膜（as-deposited）的薄膜中因孔洞引起的問題。本文首先討論自行合成的聚苯乙烯、甲基矽氧烷、以及甲基矽氧烷接枝聚苯乙烯的化學結構、基本性質，以及起始劑的含量對聚苯乙烯分子量的影響；隨後觀察孔洞大小及其影響因子，例如聚苯乙烯的分子量以及溶劑的影響；最後比較接枝形成薄膜和混摻（Hybrid）薄膜的差異。聚苯乙烯、甲基矽氧烷、以及甲基矽氧烷接枝聚苯乙烯的化學結構將由超導核磁共振光譜儀（Nuclear Magnetic Resonance Spectrometer，NMR）、紅外線光譜儀（FTIR）、以及熱重分析儀（TGA）所鑑定。聚苯乙烯、以及甲基矽氧烷接枝聚苯乙烯的熱性質可由差示熱分析儀（DSC）和熱重分析儀（TGA）取得。並用 X 光反射儀計算多孔性介電薄膜的孔隙率。最後使用掃描式電子顯微鏡觀察各式薄膜的孔洞大小及分布。

實驗結果顯示，聚苯乙烯的分子量大小受到起始劑的含量所影響，當起始劑

含量越多，則聚苯乙烯的分子量越小，進而使得薄膜形成後有較小的孔洞。併且發現，當選用和聚苯乙烯溶解係數差異較大的溶液做為溶劑時，聚苯乙烯的長鏈段會被束縛，而使得最後的薄膜有較小的孔洞。

為了證明接枝方式所製程的薄膜擁有較小的孔洞以及較佳的孔洞分布，因此，在一樣的條件下，將市售的聚苯乙烯混摻加入甲基矽氧烷溶液中，薄膜製程後可以發現會有明顯的孔洞聚集，由此可以得知，由接枝方式所製程的薄膜有效的改善了孔洞聚集的現象。

總合實驗結果可知，以接枝方式製成的薄膜其孔洞大小及分布能被有效的控制，而沒有聚集的現象產生，而孔洞大小亦受聚苯乙烯的分子量大小以及溶劑的總類所控制。綜合以上，可以確定接枝方式所製程的薄膜可被用在 ILD 層作為製作 Solid-First™ 材料更好的方式。



Novel Porous Low-k MSQ by Grafting PS-Siloxane porogen: Synthesis, Pore Morphology and Properties

Student: Shih-Ya Chiu

Advisor: Dr. Jihperng Leu

Department of Materials Science and Engineering
National Chiao Tung University

ABSTRACT

This study takes a novel approach to graft a functionalized porogen onto the backbone of low-k precursor, which is further crosslinked into a low-k matrix with well dispersed and discrete porogens to achieve excellent control of pore size and pore distribution. In particular, polystyrene (PS) is chosen as the high-temperature porogen because of its high decomposition temperature, while a widely used spin-on methylsilsequioxane (MSQ) with $k \sim 2.9$ is employed as the low k matrix in the Solid-FirstTM scheme. The high temperature porogen would be burned out after a metal/dielectric layer is completed such that the reliability issues such as insufficient barrier coverage encountered in the integration of as-deposited porous dielectrics and poor pore size/distribution could be circumvented. This study starts with the synthesis and characterization of PS-Siloxane, MSQ, and MSQ-g-PS, and then examines the relationship between the content of initiator and PS-Siloxane molecular weight. Moreover, factors for controlling the pore size such as PS molecular weight and solvent effect are investigated. Finally, we compare the pore morphology between the PS/MSQ hybrid film and MSQ-g-PS film to examine any porogen aggregation issue.

The scheme of PS-Siloxane, MSQ, and MSQ-g-PS structures are examined by $^1\text{H-NMR}$, $^{29}\text{Si-NMR}$, and Fourier-transform infrared spectroscopy (FTIR). Thermal properties such as decomposition temperature and glass transition temperature are measured by DSC and thermal gravimetric analyses (TGA). Moreover, porosity was characterized by X-ray reflectivity (XRR), while pore size was examined by scanning electron microscope (SEM).

PS-Siloxane has been synthesized by atom transfer radical polymerization (ATRP) method. It is found that PS molecular weight decreases with decreasing amount of initiator. Lower PS molecular weight (80,000 g/mole-5,000 g/mole) leads to smaller pore size in the range of 160-90 nm. Besides, adding poor solvent into MSQ-g-PS solution can limit the extending of PS long-chain, and thus reduce pore size. Compared to the MSQ/PS hybrid film, well dispersed and discrete pores have been found in MSQ-g-PS film without aggregation, which presumably enhances the mechanical strength of porous low-k films and other properties for application. Therefore, MSQ-g-PS is a novel and excellent material to be used as an ILD in Solid-FirstTM scheme.

Acknowledgements

很開心在碩士班的兩年可以在呂志鵬老師實驗室，實驗室的大家就像是一家人一樣，一起歡笑，一起努力，也很感謝老師兩年來的指導，讓我對如何研究，科技寫作，有更多的認識，也學到更多。

在此，我要謝謝國原學長這兩年來的指導，不僅是在學業，對於做人處事，以及看事情的角度更是影響我很多，跟學長聊天總是讓我能有很多收穫；謝謝幸鈴學姊幫了我好大的一個忙，如果沒有學姐，我應該還在角落掉眼淚吧；謝謝車牧龍，這兩年我從車胖身上學了很多，應對進退，以及做實驗前該先準備好的功課；還要謝謝我親愛的同學 Shindy 跟張弟，在我對材料專業領域上有不懂的地方，總是能詳細的幫我解答，最重要的事，跟他們在一起，會讓人有想往上進步的動力，也超級喜歡跟他們一起出去玩樂的。最後，謝謝大龜，泰印學長；阿義，柏村，弘恩，王智，怡臻，少農，欣源哥，狗蛋，罐頭宇，恰吉，真是的很貼心的學長姐們，不論什麼問題，他們總有專業，或是很有趣的意見，能夠有他們真是太好了；最後，還有琬婷，小白，伯政，謝謝學弟妹們總是要聽我在那邊說一些無聊的話，或是欺負他們，真是一群脾氣很好的學弟妹。最後，我要謝謝的我家人，有他們的支持，我才能一路無憂的唸到這裡，謝謝他們對我的付出。

謝謝國科會 No. 96-2221-E-009-216 的計畫，讓我在這兩年內，沒有經濟的困難，還有國家同步輻射研究中心 (NSRRC) 的光束線支援，協助我完成我的實驗。

Contents

摘要	I
ABSTRACT	III
Acknowledgements	V
Contents	VI
Table Captions	VIII
Figure Captions	IX
Chapter 1 Introduction	1
Chapter 2 Literature Review	4
2.1 Definition of low dielectric constant materials	7
2.1.1 Dielectric constant	7
2.1.2 Polarization of dielectric material	8
2.2 Requirements of low k materials for ILD applications	11
2.3 Porous low k materials	12
2.4 High-temperature porogen	15
2.5 Challenge of porous low k integration	17
2.5.1 Mechanical strength	17
2.5.2 Porosity versus modulus	18
2.5.3 Moisture uptake	20
2.5.4 Cu diffusion	21
2.6 Living radical polymerization	23
2.6.1 Atom Transfer Radical Polymerization (ATRP)	24
2.6.2 Stable Free-Radical Polymerization (SFRP)	26
2.6.3 Radical Addition-Fragmentation Transfer (RAFT)	27
2.7 Cross-linking of siloxane	28
2.8 Characterization Methodologies	29
2.8.1 Nuclear Magnetic Resonance Spectroscopy (NMR)	29
2.8.2 Gel Permeation Chromatography (GPC)	30
2.8.3 Different Scanning Calorimetry (DSC)	31
2.8.4 Thermal Gravimetric Analysis (TGA)	32
2.8.5 Fourier-transform infrared spectroscopy (FTIR)	33
2.8.6 Scanning Electron Microscope (SEM)	34
2.8.7 X-ray reflectivity (XRR)	35
Chapter 3 Experimental	37
3.1 Materials	37
3.1.1 Chemicals	37
3.1.2 Matrix	39

3.1.3 Solvent	39
3.1.4 Acid	40
3.2 Preparation	41
3.2.1 Purification of styrene (St) and CuBr(I)	41
3.2.2 Synthesis of α -siloxane-polystyrene (PS-siloxane)	41
3.2.3 Synthesis of MSQ from MTMS using sol-gel	42
3.2.4 Grafting PS onto MSQ through siloxane-PS	42
3.2.5 Preparation of porous low-k film	42
3.2.6 Solvent effect on the pore size of porous low-k films	42
3.3 Experimental techniques	43
3.3.1 Nuclear Magnetic Resonance Spectroscopy (NMR)	43
3.3.2 Gel Permeation Chromatography (GPC)	43
3.3.3 Different Scanning Calorimetry (DSC)	43
3.3.4 Thermal Gravimetric Analyses (TGA)	43
3.3.5 Fourier-transform infrared spectroscopy (FTIR)	44
3.3.6 Scanning Electron Microscope (SEM)	44
3.3.7 X-ray reflectivity (XRR)	44
Chapter 4 Results and Discussion	45
4.1 Synthesis and properties of PS-siloxane	45
4.1.1 Synthesis of PS-siloxane	45
4.1.2 Thermal properties of PS-Siloxane	49
4.2 Synthesis of MSQ	51
4.3 Grafting PS-siloxane onto MSQ	53
4.4 Pore morphology of MSQ-g-PS porous low k film	59
4.4.1 The relationship between molecular weight and pore size in MSQ-g-PS	59
4.4.2 Solvent effect	63
4.4.3 Porosity	70
4.5 Comparison between MSO-g-PS and MSQ/PS hybrid porous low k films ..	72
Chapter 5 Conclusion	74
References	76

Table Captions

Table 2. 1 Requirements of low k materials for ILD application	11
Table 2. 2 Opening temperatures of key backend processing steps.....	16
Table 3. 1 The recipe of ATRP reaction for various PS molecular weight.....	42
Table 4. 1 Primary absorption peak position and their assignment.....	52
Table 4. 2 peak assignment of ^{29}Si -NMR spectra.....	58
Table 4. 3 Parameters of $R=a(M)^b$ for various solvents.....	68
Table 4. 4 Solubility parameters for various solvents.....	69
Table 4. 5 Calculation of density and porosity	71



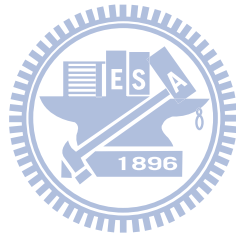
Figure Captions

Figure 1. 1 Interconnect pore and pore distribution due to aggregation in MSQ/PS-b-P4VP hybrid film	2
Figure 2. 1 Structures of multilayer interconnect (a) Al metallization, and (b) Cu metallization.....	4
Figure 2. 2 Schematic diagram of a typical interconnect element.....	5
Figure 2. 3 Relationship between generation node and RC delay in gate and interconnect for Al/SiO ₂ and Cu/low k.....	6
Figure 2. 4 Capacitor with dielectric.....	8
Figure 2. 5 Electronic polarization.....	9
Figure 2. 6 Ionic polarization.....	9
Figure 2. 7 Orientation polarization.....	10
Figure 2. 8 Relationship between dielectric constant and applied electric fieldfrequency	11
Figure 2. 9 Procedure of sol-gel.....	13
Figure 2. 10 Mechanism of NSC method	14
Figure 2. 11 General processing scheme to produce nanoporous structure using templating method.....	15
Figure 2. 12 Morphologies of template structures	16
Figure 2. 13 Morphology of worm pore and interconnect pore.....	17
Figure 2. 14 Delamination during CMP process.....	18
Figure 2. 15 Porosity versus modulus.....	19
Figure 2. 16 Pore size versus mechanical strength with the same porosity.....	20
Figure 2. 17 Damage of dielectric layer by solvent.....	21
Figure 2. 18 Copper deposited into dielectric layer.....	22

Figure 2. 19 Solid-First TM scheme	23
Figure 2. 20 Mechanism of living radical polymerization (LRP).....	24
Figure 2. 21 Mechanism of ATRP.....	25
Figure 2. 22 Block copolymer mechanism of ATRP	26
Figure 2. 23 the thermal decomposition of an alkoxyamine into a reactive radical and a stable radical.....	26
Figure 2. 24 Mechanism of SERP.....	27
Figure 2. 25 Mechanism of RAFT	27
Figure 2. 26 Condensation reaction in the siloxane cross-linking.....	28
Figure 2. 27 Sol gel MTMS to MSQ	29
Figure 2. 28 Diagram of GPC	31
Figure 2. 29 Schematic of a heat flux DSC cell.....	32
Figure 2. 30 Components of a thermal balance: A: beam, B: sample cup and holder, C: counterweight, D: lamp and photodiodes, E: coil, F: magnet, G: control amplifier, H: tare calculator, I: amplifier, J: recorder.	33
Figure 2. 31 Schematic diagram of a FIB/SEM system.....	35
Figure 2. 32 Kieddig interference fringe.....	36
Figure 4. 1 Synthesis scheme of siloxane-polystyrene.....	46
Figure 4. 2 ¹ H-NMR spectrum of siloxane-PS	46
Figure 4. 3 PS molecular weight as a function of initiator weight loading	48
Figure 4. 4 TGA of PS-Siloxane	50
Figure 4.5 DSC curve of PS-siloxane.....	51
Figure 4. 6 The schematic of MSQ synthesis from MTMS monomers.....	52
Figure 4. 7 FTIR spectra of MSQ cured at 60 °C and 400 °C.....	53
Figure 4. 8 Schematic reaction diagram of grafting PS onto MSQ through siloxane-PS	54

Figure 4. 9 TGA data of MSQ and PMS-g-PS.....	55
Figure 4. 10 Derivative of TGA data of MSQ	55
Figure 4. 11 Derivative of TGA data of MSQ-g-PS	56
Figure 4. 12 IR spectra of MSQ-g-PS.....	57
Figure 4. 13 TDS of CH ₄ for where CH ₄ evolution data of MSQ	57
Figure 4. 14 ²⁹ Si-NMR of MSQ-g-PS.....	58
Figure 4. 15 SEM photograph of MSQ-g-PS porous low k film (MW of PS: 80,000 g/mole).....	60
Figure 4. 16 SEM photograph of MSQ-g-PS porous low k film (MW of PS:10,000 g/mole).....	61
Figure 4. 17 SEM photograph of MSQ-g-PS porous low k film (MW of PS: 5,000 g/mole).....	61
Figure 4. 18 SEM of MSQ-g-PS low k films with various MWs: (a) 80,000 g/mole (b) 10,000 g/mole (c) 5,000 g/mole.....	62
Figure 4. 19 Pore size as a function of the square root of PS molecular weight	62
Figure 4. 20 PS <i>M_w</i> : 80,000 g/mole, solvent was Ethanol/THF	64
Figure 4. 21 PS <i>M_w</i> : 80,000 g/mole, solvent was n-Hexane/THF	64
Figure 4. 22 PS <i>M_w</i> : 10,000 g/mole, solvent was Ethanol/THF	65
Figure 4. 23 PS <i>M_w</i> : 10,000 g/mole, solvent was n-Hexane/THF	65
Figure 4. 24 PS <i>M_w</i> : 5,000 g/mole, solvent was Ethanol/THF	66
Figure 4. 25 PS <i>M_w</i> : 5,000 g/mole, solvent was n-Hexane/THF	66
Figure 4. 26 Summary of pore morphology and pore size	67
Figure 4. 27 Solvent effect of pore size	68
Figure 4. 28 The mechanism of PS activity in good solvent or in poor solvent.....	70
Figure 4. 29 Morphology of MSQ/PS hybrid porous low k film	73
Figure 4. 30 Morphology of (a)MSQ/PS hybrid porous low k film (PS <i>M_w</i> :90,000	

g/mole) and (b) MSQ-g-PS porous low k film (PS M_w :80,000 g/mole)..... 73



Chapter 1 Introduction

To overcome the increase of RC delay due to the scaling of integrated circuit devices [1], scientists and engineers developed two major solutions for the backend interconnect: first was copper metallization using a dual damascene architecture, and the second was low dielectric constant (low k) materials [2] such as carbon-doped oxide or SiLK™ [3] ($k \sim 2.6-3.0$) in the past decade. For ultra-low k materials ($k < 2.5$) in 45nm node and beyond, pores at various porosity have been incorporated into the dielectric matrix to reduce k-value. Most of ultra-low k films were made by introducing templating agent [4] into silica structure using spin-on solution coating or plasma-enhanced chemical vapor deposition (PE-CVD). The templating agent or pore generator (porogen) was then removed during the deposition or subsequent thermal process. However, due to large pore size/distribution or interconnected pores, porous low k films faced some critical issues such as (1) low mechanical strength leading to delamination or cracks after chemical-mechanical polish (CMP) or packaging and (2) poor barrier/dielectric reliability due to non-continuous side-wall coverage of barrier. In 2003, Shipley Inc. introduced a solution, “Solid-First™” scheme [5] to circumvent these issues. Solid-First™ uses a high-temperature porogen and new integration scheme, which defers the formation of porous dielectric, *i.e.* the removal of high-temperature porogen after a metal/low-k layer is completed.

The common method for preparing porous low k films based on the Solid-First™ scheme is to mix the high-temperature porogen into a silica-containing matrix such as spin-on glass in a solution, then spin-coat the matrix/porogen solution onto a substrate, which is followed by a cure step preferably at ≤ 300 °C to form a crosslinked dielectric with high-temperature porogen as the starting interlayer dielectric (ILD) for

subsequent dual damascene integration flow. However, serious reliability concerns such as poor size distribution and/or interconnected pores, as illustrated in Fig. 1.1 [6], results were from enhanced diffusion and porogen aggregation [7] during the cure step [8]. For examples, such large pore size and interconnected pores may detrimentally degrade the ultra-low-k film's mechanical strength [9] such that it cannot meet the minimum requirements (~ 4 GPa) for applications in the copper/low-k backend interconnect. For matrix/high-temperature porogen hybrid system (MSQ/polystyrene), recent efforts such as fast heating rate in the cure step or controlling the zeta-potential of polystyrene porogen by pH values or surfactants in the solution have successfully reduce the pore sizes and distribution down to 100 nm [10,11]. Yet, there is still room for improvement in terms of the pore size and especially the distribution, especially for ultra-low-k materials with high porosity > 40-50%.

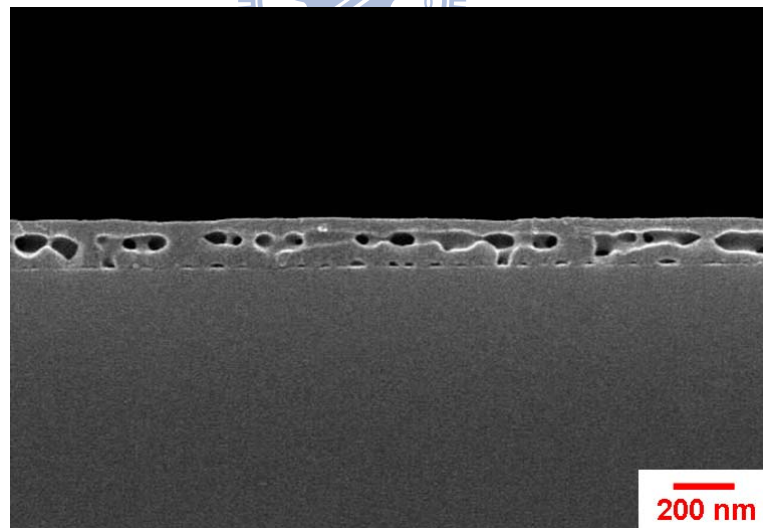


Figure 1. 1 Interconnect pore and pore distribution due to aggregation in MSQ/PS-b-P4VP hybrid film

In order to circumvent the issues of large pore sizes, interconnected pores, and poor distribution in a matrix/porogen hybrid system caused by severe aggregation of

porogen during the cure process, this study takes a novel approach by grafting a functionalized porogen onto the backbone of low-k precursor, which is further crosslinked into a low-k matrix with well dispersed and discrete porogen to achieve excellent control of pore size and pore distribution. In particular, polystyrene (PS) is chosen as the high-temperature porogen because of its high decomposition temperature, while a widely used spin-on methylsilsesquioxane (MSQ) with $k \sim 2.9$ is employed as the matrix. However, there are a couple of problems to be fixed first: (1) polystyrene does not have the functional group as the grafting agent for this study, and (2) commercial MSQ does not dissolve in THF. As a result, polystyrene (PS) with a $-\text{CH}_2-\text{CH}(\text{Ph})-\text{C}_3\text{H}_6-\text{Si}(\text{OCH}_3)_3$ siloxane functional group, which can be grafted onto MSQ precursor as a templating porogen, are first synthesized in this study. Furthermore, MSQ is freshly prepared from methyl-trimethoxy silane (MTMS) monomer by sol-gel method, which can be then dissolved in THF. The as-prepared PS-grafted MSQ is named MSQ-g-PS for simplicity throughout the rest of this thesis.

In this thesis, the synthesis and characterization of PS-siloxane, MSQ and MSQ-g-PS will be first carried out. The relationship between the content of initiator and PS molecular weight in PS-siloxane will be further investigated. The structure properties of porous low k film based on MSQ-g-PS, such as pore size, porosity, and morphology will be examined. The factors for controlling pore size such as PS molecular weight and solvent effect are also studied. Finally, comparison between the PS/MSQ hybrid film and the MSQ-g-PS film is made to examine any improvement in pore size/distribution.

This thesis included five chapters: Chapter 1 Introduction, Chapter 2 Literature Review, Chapter 3 Experimental, Chapter 4 Results and Discussion, and Chapter 5 Conclusion.

Chapter 2 Literature Review

For past 45 years, integrated circuit (IC) dimensions continue shrinking towards small size according to Moore's Law [12]. Modern integrated circuit devices contain millions of transistor electrically connected by millions of wires fabricated on the top of transistors. The wires, or "interconnect", transform transistors into a functioning device by local, semi-global and global wire layout. In 65 nm node, device has as many as 9-10 layers of interconnect which was so called multilayer interconnect. Typically, multilayer interconnect was fabricated using Al or Cu as the conductor and SiO_2 as the dielectric. Figure 2.1 [13] shows structures of interconnect (a) Al metallization, and (b) Cu metallization

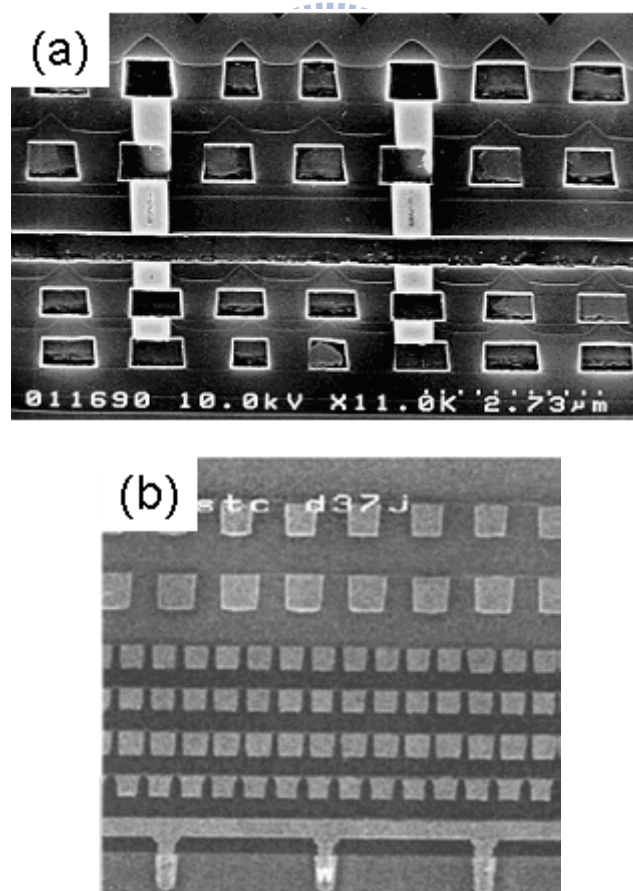


Figure 2.1 Structures of multilayer interconnect (a) Al metallization, and (b) Cu metallization

When IC dimensions continue to decrease, RC delay, crosstalk noise and power dissipation of the interconnect structure would become problems for ultra-large-scale integration (ULSI) of IC. Figure 2.2 shows a schematic diagram of a typical element in multilevel interconnects, where P represents line pitch, W the metal line width, S the spacing between line to line, T the thickness of metal line.

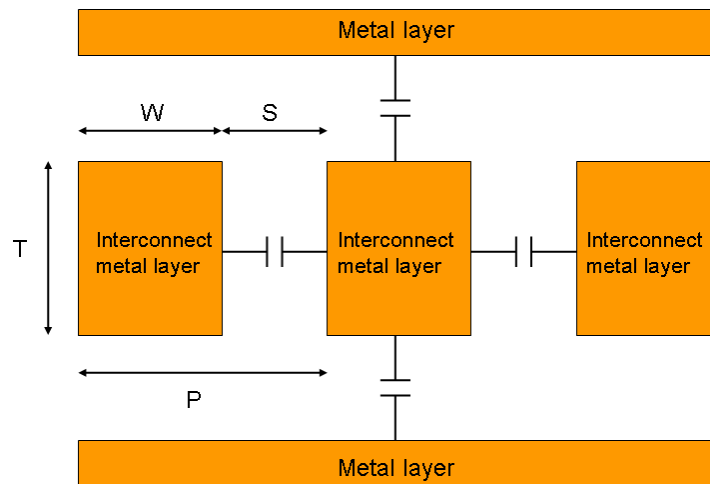


Figure 2. 2 Schematic diagram of a typical interconnect element.

RC delay can be calculated using a simple first-order model as Equation 2.1

$$RC = 2\rho\kappa\epsilon_0 \left(\frac{4L^2}{P^2} + \frac{L^2}{T^2} \right) \quad (2. 1)$$

where

ρ : metal resistivity

ϵ_0 : the vacuum permittivity

κ : the relative dielectric constant of dielectrics

L: the length of the metal line

There are two sets of parameters could determine RC delay such as (1) material properties including the metal resistivity ρ and the dielectric constant κ , and (2) interconnect dimensions. Figure 2.3 shows relationship between generation node and RC delay in gate and interconnect for Al/SiO₂ and Cu/low k [14]. As IC scaling proceeds beyond the 250 nm node, the interconnect delay will exceed the gate delay [15].

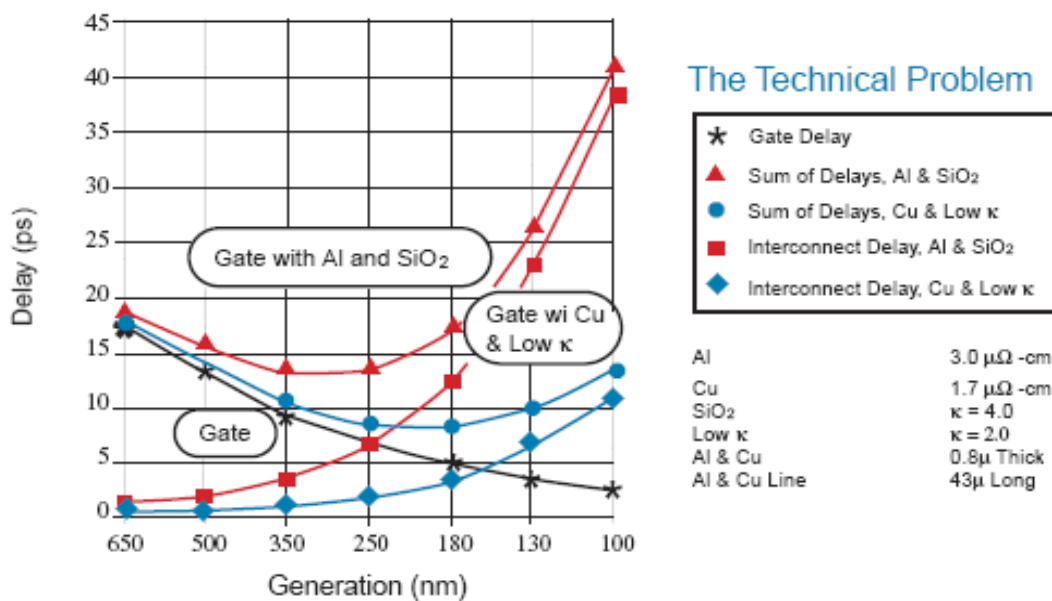


Figure 2. 3 Relationship between generation node and RC delay in gate and interconnect for Al/SiO₂ and Cu/low k

In order to solve RC delay issues, new materials with lower resistivity and dielectric constant have been developed and introduced to semiconductor widely. Cu (1.9 $\mu\Omega$ cm) replaced Al(Cu) (3.3 $\mu\Omega$ cm) in interconnect metallization [16]. There is another way can improve RC delay effectively, switching SiO₂ to a low k ILD with a

κ of about 3.0 [17].

The early adoption of low k preferred the modification of silicon oxide such as fluorinated silicate glass (FSG) with κ of about 3.5~3.7, then carbon-doped oxide with κ of about 2.5~3.2. κ value of dense carbon-doped oxide has a lower limit at 2.5-2.6 [18]. In addition to integration of porous material through many different backend processes models, the most important task is to design the low k material in the matrix and porogen to alleviate the subsequence relatively or process issue. However, porous low k may encounter reliability issues such as (1) low mechanical strength, delamination and cracks during CMP [19], and (2) Un-continue barrier coverage at the trench side-wall [20].

For porous low k material, it is desirable to have small pores, tight distribution, in well dispersed and closed-cell form at the same porosity. A study of how to solve issues of porous low k materials encounter is the most important task in the backend technology of 45 nm node and beyond. There, in corporation of porosity to achieve low k material with $\kappa < 2.5$ become necessary [21].

2.1 Definition of low dielectric constant materials

2.1.1 Dielectric constant

For a parallel-plate capacitor with dielectric as shown in Figure 2.4, the capacitance C_0 of a capacitor can be expressed by Equation 2.2, where Q represent charge and V represents voltage, A is electrode area of a parallel-plate, d is distance between the parallel-plate, ϵ is the permittivity of substance, and ϵ_0 is vacuum permittivity (8.85×10^{-12} F/m).

$$C_0 = \frac{Q}{V} = \epsilon \frac{A}{d} = \kappa \epsilon_0 \frac{A}{d} \quad (2.2)$$

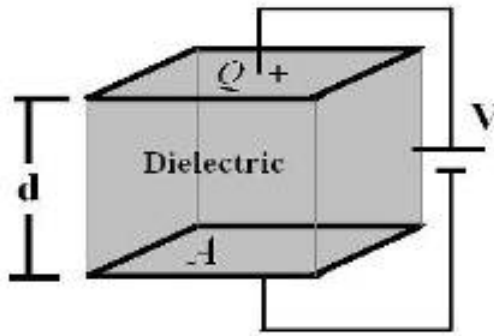


Figure 2. 4 Capacitor with dielectric

Dielectric constant (κ) is a frequency dependent and composed of electronic, atomic, and dipole orientational contributions [22,23].

2.1.2 Polarization of dielectric material

When a dielectric is placed between charged parallel-plate, the polarization of the medium produces an electric field opposing the field of the charges on the plate. The electric field would induce an electric dipole, and redistribution of positive and negative charges was called polarization. Material which contains polar molecules would be in random orientations when no electric field is applied. The dipole moment of the polar material would be polarized when electric field is applied. The dipole moment in unit volume represented the degree of polarization called polarization strength.

There are four styles of polarization such as electronic polarization, ionic polarization, orientation polarization, and space charge [24]. A neutral atom has electron cloud around its nucleus, the electric density would change when the outside electric field displaces. Outer atom electron and inter proton in materials in an electric

field was called electronic as shown in Figure 2.5. Moreover, atomic polarization is defined when the electronic cloud is deformed under the force of the applied field, so the negative and positive charge are formed. Atomic polarization was also called Electronic polarization.

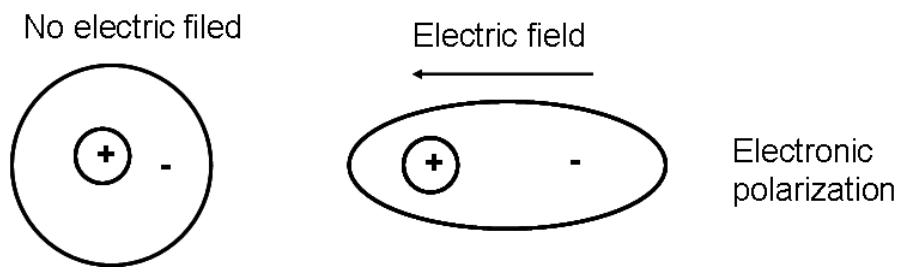


Figure 2. 5 Electronic polarization



Positive and negative ions in ionic crystals such as NaCl were displaced when electric field was applied. The phenomenon was called ionic polarization as shown in Figure 2.6.

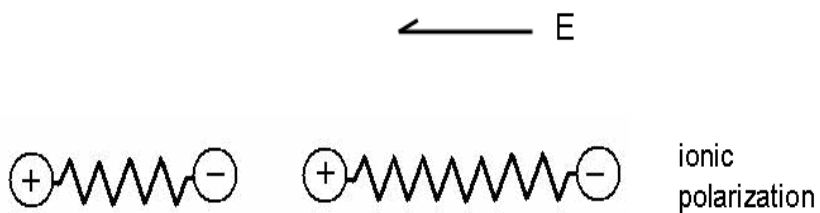


Figure 2. 6 Ionic polarization

A material was with built-in dipoles which were independent of each other. After electric field was applied, and only induced a little bit of average orientation in field direction. This phenomenon so call orientation polarization as shown in Figure 2.7.

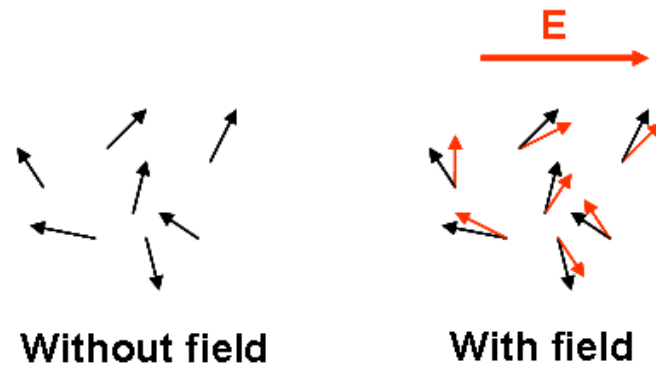


Figure 2. 7 Orientation polarization

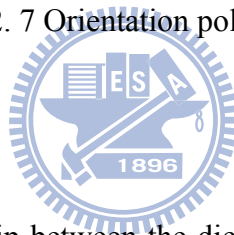


Figure 2.8 shows relationship between the dielectric properties of materials and operation frequency. The frequency which was contributed by electronic, atomic and orientation polarization related with dielectric constant [25]. Electronic polarization was the primary contribution at the optical frequency, because atomic and orientation can not respond so fast.

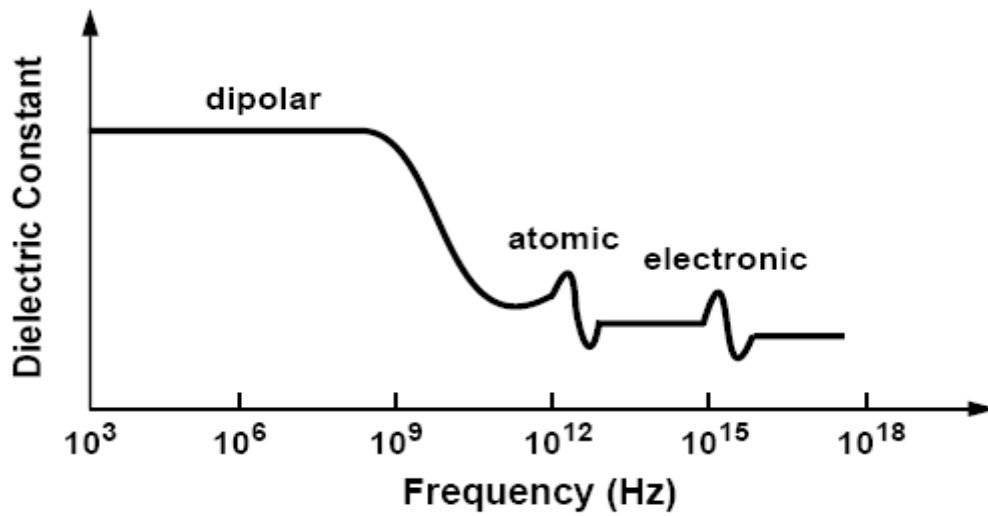


Figure 2. 8 Relationship between dielectric constant and applied electric field frequency

2.2 Requirements of low k materials for ILD applications

Materials which were used in ILD needed not only decreased dielectric constant but also excellent mechanical strength, low moisture, and thermal stability etc. Table 2.1 [26] summarized the requirements of low k materials which were applied in ILD.

Table 2. 1 Requirements of low k materials for ILD application

Electrical	Chemical	Mechanical	Thermal
Low dielectric constant	Good chemical resistance	Thickness uniformity	High thermal stability
Isotropic	Low moisture uptake <1%	Good adhesion	CTE <50 ppm/°C
Low dissipation	Etch rate and selectivity	Residual stress <100Mpa	Low thermal shrinkage
Low leakage current	Low gas permeability	Crack resistance	High thermal conductivity
Low charge trapping	No metal corrosion	Tensile modulus	
High electric field strength			

2.3 Porous low k materials

Recently, low k material which had dielectric constant at 2.6~2.9 was widely used in 0.65 μm technology node. However, future technology nodes would need lower dielectric constant. Porous materials was announced to decrease dielectric constant, which incorporated air ($\kappa=1$) into matrix. Porosity can be affected by the volume fraction of air which related with pore size, shape, and distribution. There were some methods to manufacture porous low k material such as sol-gel method, nano-clustering method, and templating method.

(1) Sol-gel method

Inorganic glasses were modified to become polysiloxane [27] using sol-gel method. Sol-gel procedure involved (1) hydrolyzing silicon alkoxides, and (2) copolymerizing the hydrolyzate with a hydroxyl-terminated polysiloxane. Figure 2.9 shows the procedure of sol-gel [28]. In porous low k material, colloids were dispersed in solvent, and then the reaction would form 3-dimension network structure. During drying process, the liquid was replaced with air. Pore size was un-controllable using sol-gel method.

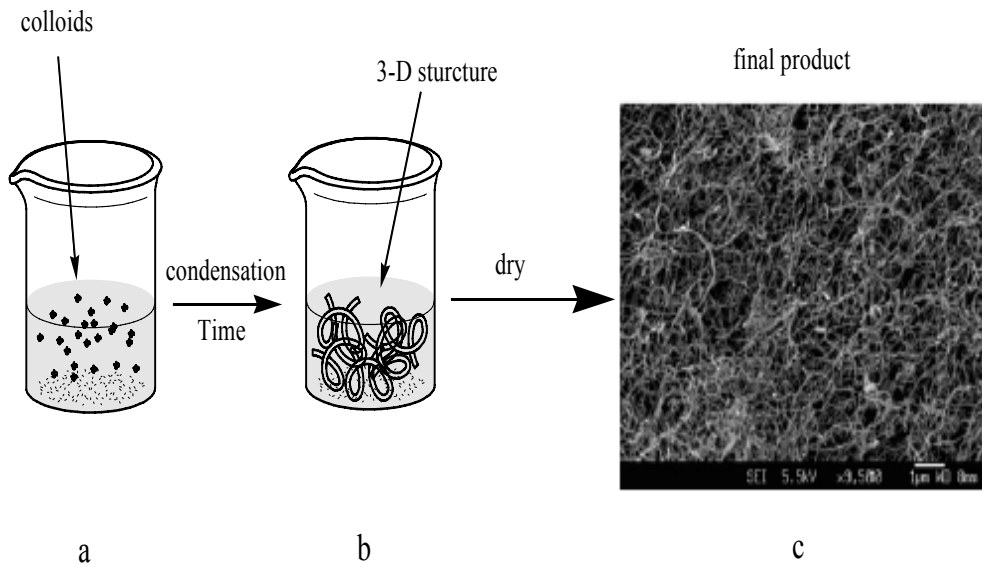


Figure 2. 9 Procedure of sol-gel

(2) Nano-clustering silica (NCS) method

NCS mixed silica source monomer and particular compounds such as amine or PTAOH in a solvent. The silica source monomers would hydrolyze and get around with compounds, and make small size clusters. Cluster would polymerize in thermal heating process. Silica clusters were cured to keep pore situated in the silica cluster. Mesopore among the silica clusters were formed. Figure 2.10 [29] shows the mechanism of NCS method.

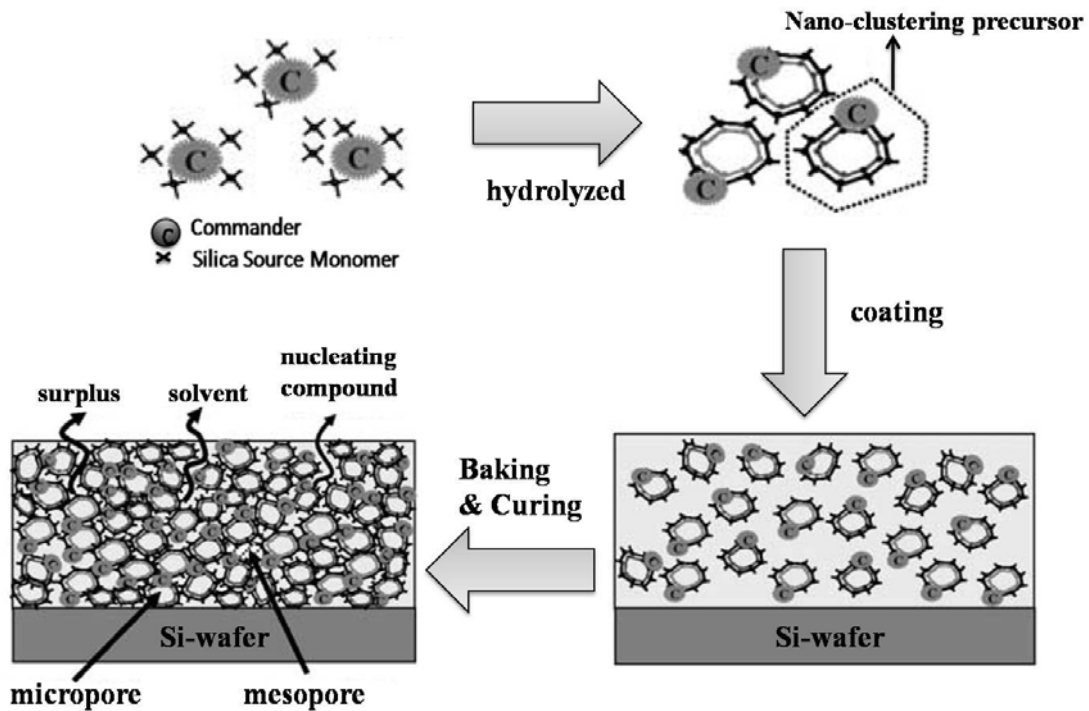
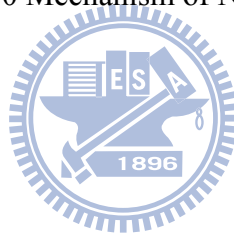


Figure 2. 10 Mechanism of NSC method



(3) Template method

Templated polymerization has been used in monomeric and polymeric surfactants [30]. Porous structure can be quite regulated in silica phase. The templated polymerization was affect on the continuous formation of a variety of self-assembled structures and strong interactions between these structures and the vitrifying medium. Surfactants were removed in curing process, and would have porous structure in silica phase. There were three steps of templated polymerization: (1) synthesis, (2) drying, (3) template removal. Figure 2.11 [31] shows the general processing scheme to produce nanoporous structure, where stage 1 was templated resin polymerization, and stage 2 was porogen decomposition.

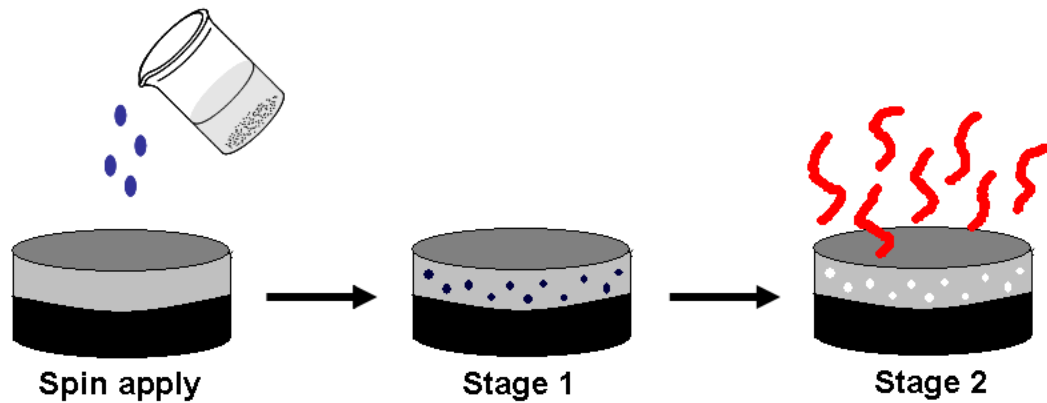


Figure 2. 11 General processing scheme to produce nanoporous structure using templating method

2.4 High-temperature porogen

Template has been used for a long time, and the microstructure of template materials could be disorder [32] and order which included lamellar [33], cubic [34] or hexagonal [35] structure as shown in Figure 2.12. The interaction of surfactant (S) and inorganic matrix (I) would cause the difference of structure. The interaction include electrostatic [36], hydrogen bonding [37], hydrogen bonding/ electrostatic [38], covalent [39]. However, the surfactant (ammonium) and matrix (silica) were toxic, expensive, and impractical for used in IC industries. Table 2.2 shows the upper opening temperature of the backend processing step. Therefore, the decomposition temperature of high-temperature porogen should higher than 300 °C. Order templates have been studied for a long time, but disorder templates which were controllable and easy making, have been widely used in the preparation of low k materials. The conventional method of making spin-on during the cure low k material was hybrid porogen into matrix. However, porogen would aggregate and to mix porogen into matrix to form a hybrid system to pore aggregation on the thin film. In order to solve this problem, “Grafting the porogen onto matrix” was proposed. The grafting method for functionalized porogen will be reviewed in the next section 2.6.

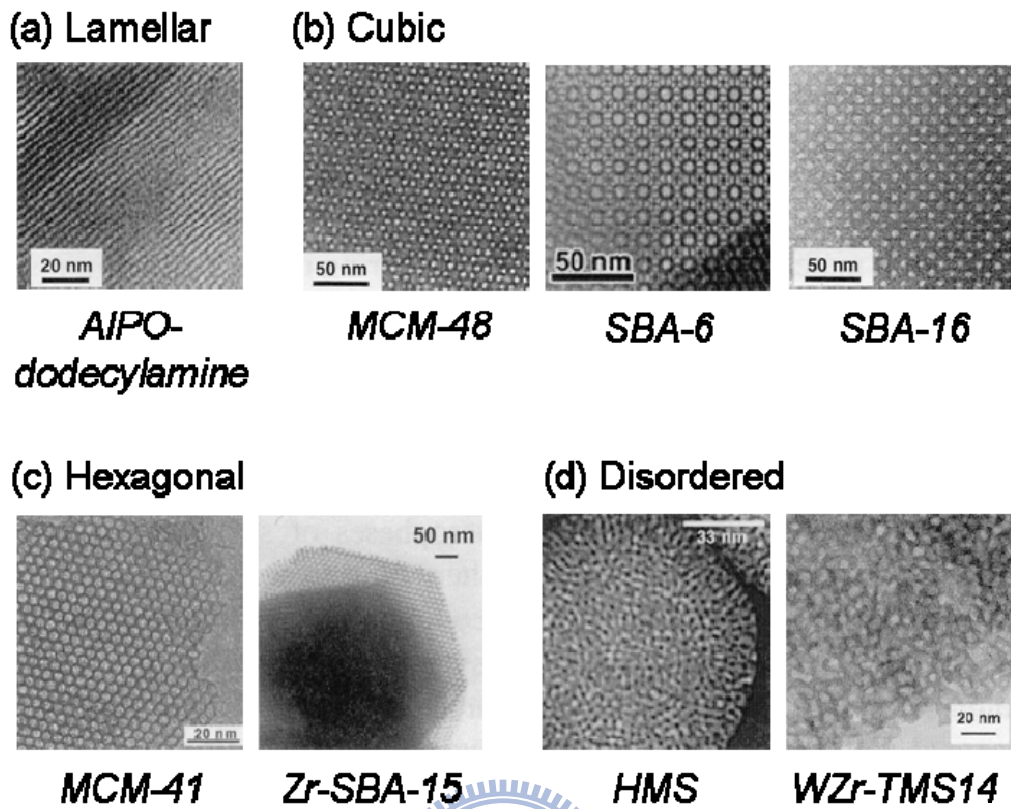


Figure 2. 12 Morphologies of template structures

Table 2. 2 Opening temperatures of key backend processing steps

Processing step	Upper limit (°C)	Solid-First™ (°C)
ILD deposition or cure	400	250~300
Lithography	< 160	< 160
Plasma etching	< 150	30 (RIE N ₂ H ₂)
Wet clean	<100	< 100
Barrier/seed deposition	< 250	< 100
Electroplating	< 70	< 100
Annealing (Cu or low-k)	300	150
CMP	R.T.	R.T.
SiN ES depositon	400	

2.5 Challenge of porous low k integration

Porous low k materials have lower dielectric constant than traditional silicon dioxide. However, there were some disadvantages of porous low k film such as weaker mechanical properties and chemical resistance.

2.5.1 Mechanical strength

Pore aggregation caused low mechanical strength, and led to dielectric layer can not survive under chemical mechanical polish (CMP) process [40]. Figure 2.13 shows the worm pore which was caused by pore aggregated [6], and Figure 2.14 shows the delamination during CMP process [10].

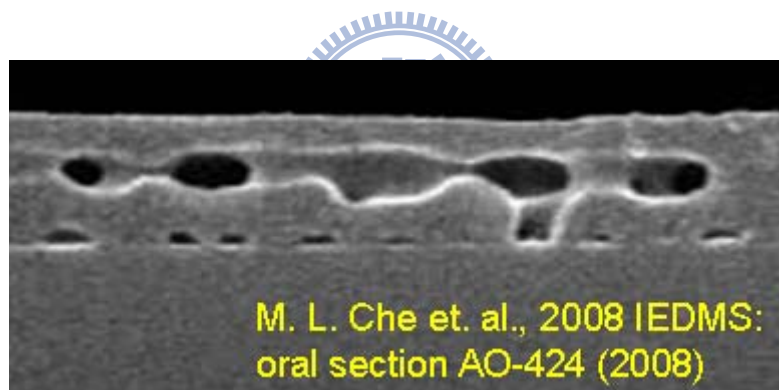


Figure 2. 13 Morphology of worm pore and interconnect pore

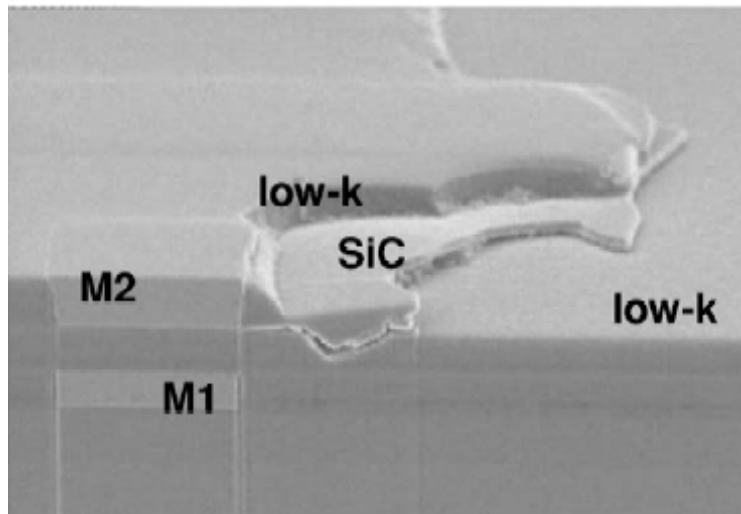


Figure 2. 14 Delamination during CMP process

2.5.2 Porosity versus modulus

Modulus decreased rapidly with increasing porosity [41] as described by Equation 2.3 [42]. These values were similar to those measured for other porous materials with irregularly shaped pores. This was reasonable because the nature of the phase-separation mechanism used to generate pores in materials provides isotropic porous structures with random morphology [43,44]. Figure 2.15 shows the relationship between porosity and modulus [45].

$$E_f = E_0(1 - aP)^n \quad (2.3)$$

Where

E_f = modulus of thin film

E_0 = modulus of the matrix

P = porosity

a and n = material constants

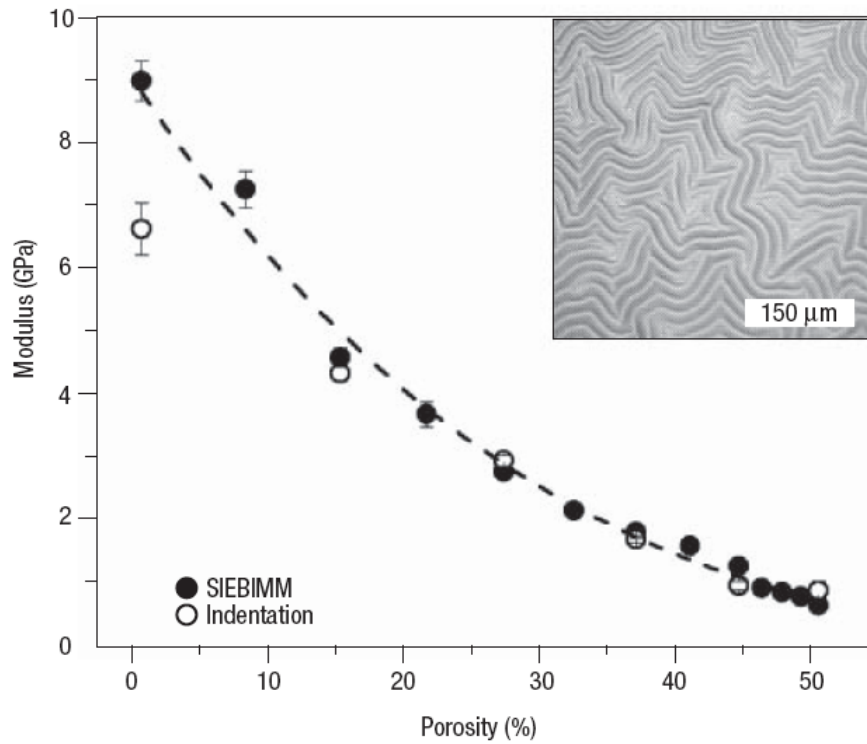


Figure 2. 15 Porosity versus modulus

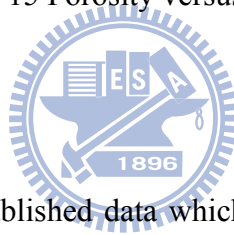


Figure 2.16 shows the unpublished data which produced by NIP Lab in NCTU [11]. In the same porosity condition, thin film which has smaller pore would have higher mechanical strength. Large pore decreased strength of thin film. For highly porous low k films, it is desirable to have small pore size at even high porosity in order to retain a better mechanical strength.

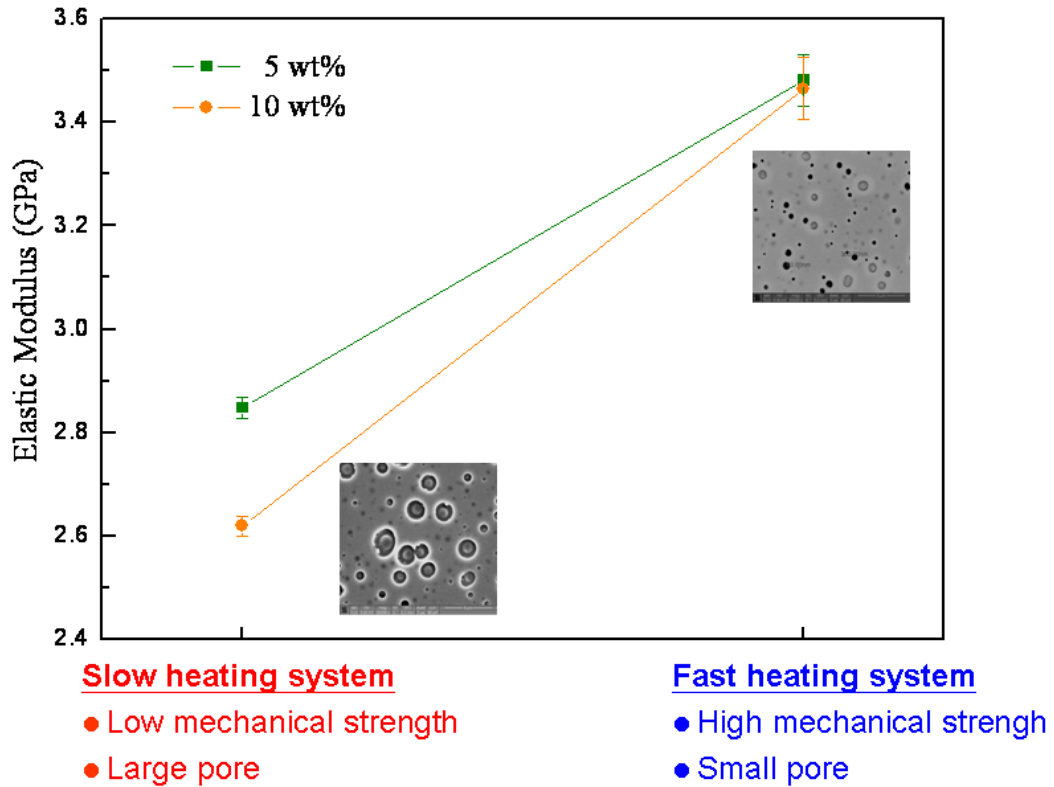
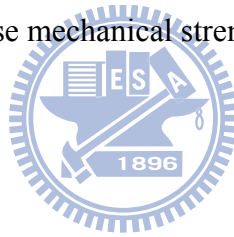


Figure 2. 16 Pore size verse mechanical strength with the same porosity



2.5.3 Moisture uptake

Porous low k may absorb moisture in wet etching, wet cleaning, or resist cleaning processing steps, and lead to dielectric constant increase ($\kappa_{\text{water}} \sim 80$). Besides, low k film could be destroyed by solvent in manufacture process if its chemical resistance is poor. Figure 2.17 shows the damage of dielectric layer by solvent [10].

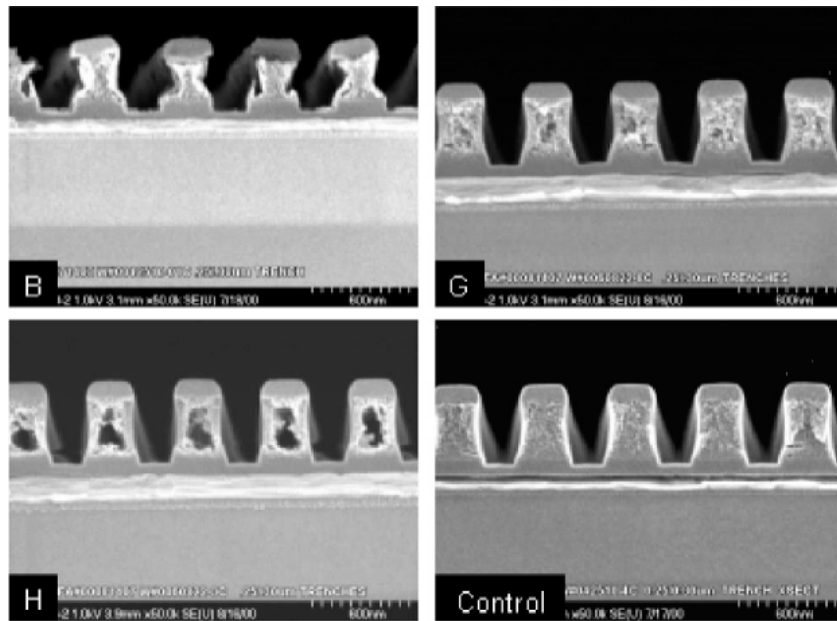
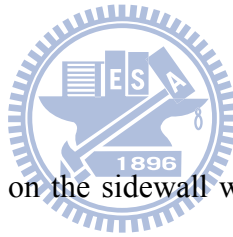


Figure 2. 17 Damage of dielectric layer by solvent

2.5.4 Cu diffusion

In the etching process, pore on the sidewall would be etched and become open pore, which may result in non-continuous sidewall. The barrier can not protect low k layer completely. Copper may diffuse into low k layer and destroyed the function of low k layer [46]. This damage would increase leakage and decrease breakdown voltage, and lead to circuit failure. Figure 2.18 shows copper diffused into dielectric layer.



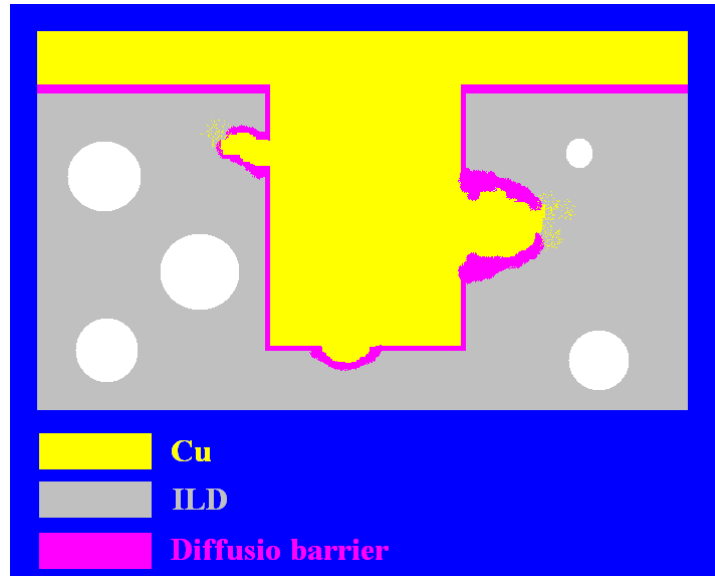


Figure 2. 18 Copper deposited into dielectric layer

In order to solve these problems, Shipley Company announced a Solid-First™ scheme which can eliminate the problem of non-continuous barrier coverage and ensured dielectric layer can survive under CMP process. The procedure of Solid-First™ scheme included (1) high-temperature porogen and silicon matrix were deposited, (2) patterning steps such as lithography, etch, and clean, (3) metallization and CMP, and (4) removed high-temperature porogen at 300~400 °C. The decomposition temperature of high-temperature porogen should higher than 300 °C, while the common temperature of backend processing under than 300 °C. Figure 2.19 shows the processing step in Solid-First™ scheme.

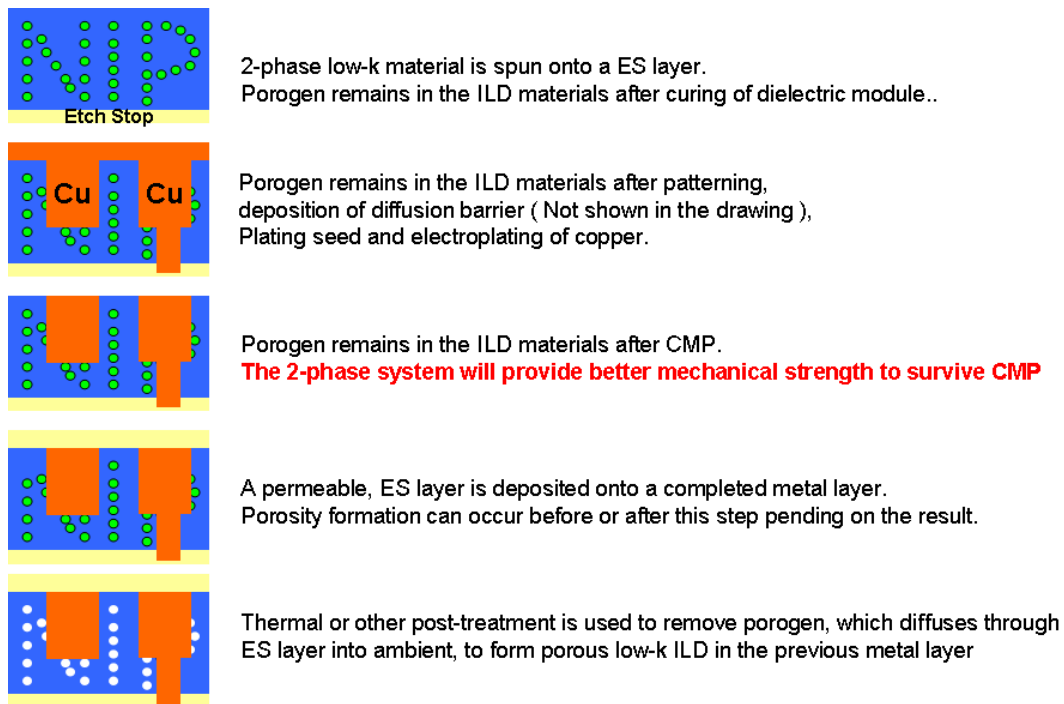
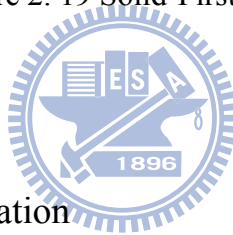


Figure 2. 19 Solid-First™ scheme



2.6 Living radical polymerization

General Considerations

Conventional chain polymerization systems, both of radical and ionic would break molecule chains. In contrast chain polymerization without chain-breaking reactions is living radical polymerization (LRP). LRP allowed the synthesis of block copolymer. The situation was very different for conventional (nonliving) radical polymerization since the lifetime of radicals was very short [47]. Compared with ionic polymerization, LRP have good commercial potential for materials synthesis. Figure 2.20 shows the mechanism of living radical polymerization, where RZ is initiator and M is monomer.

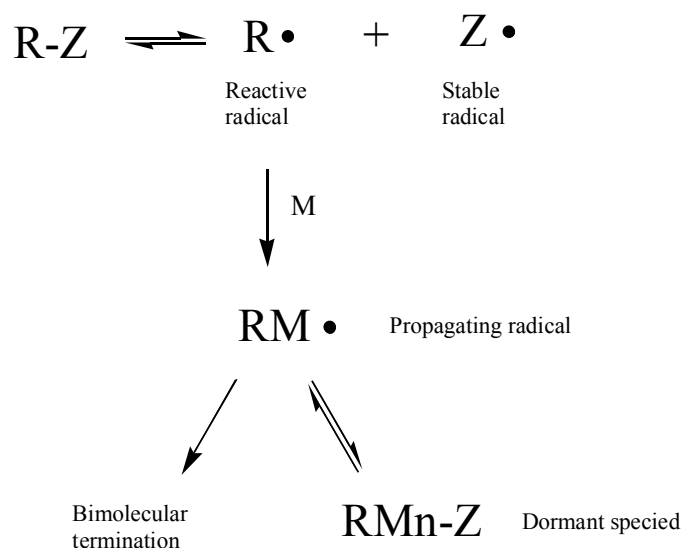


Figure 2. 20 Mechanism of living radical polymerization (LRP)

In general living radical polymerization included atom-transfer radical polymerization (ATRP), stable free-radical polymerization (SFRP), and reversible addition-fragmentation transfer (RAFT). Both of ATRP and SFRP proceed with reversible termination, but RAFT proceed with reversible chain transfer.

2.6.1 Atom Transfer Radical Polymerization (ATRP)

Atom-transfer radical polymerization (ATRP) involved an organic halide undergoing a reversible redox process catalyzed by a transition metal compound such as cuprous halide [48]. Figure 2.21 shows the mechanism of ATRP, where RBr is initiator, CuBr is catalyzed, L is ligand, and M is monomer. Ligand could combine with cuprous salt and solubilize cuprous salt in the organic reaction system.

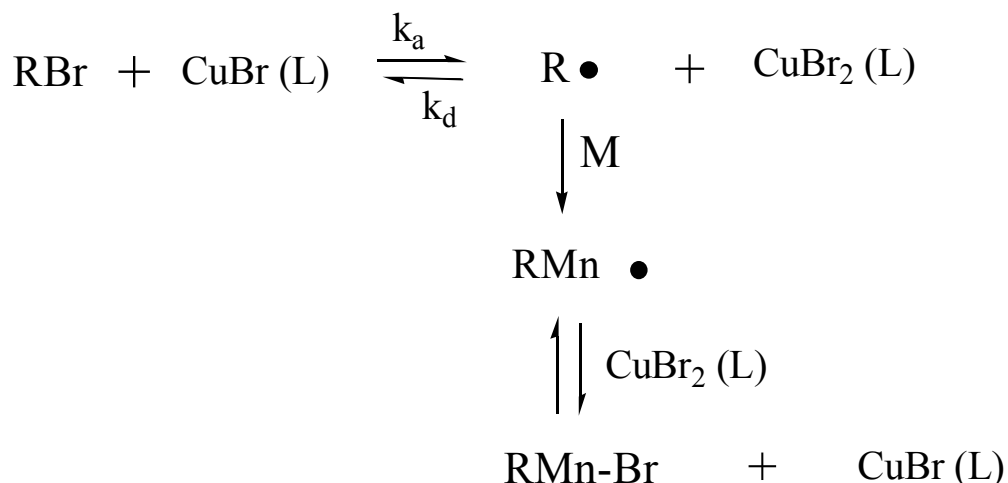


Figure 2. 21 Mechanism of ATRP

ATRP reactivity was related with monomer, metal catalyst, organic halides, temperature, and solvent. A number of different types of copolymers can be prepared by ATRP such as statistical (random), gradient, block, and graft copolymers [49]. Block copolymers have been synthesized via ATRP by two methods: (1) one-pot sequential, and (2) isolated macroinitiator [50]. Figure 2.22 shows the block copolymer mechanism of ATRP. AB diblock copolymer is synthesized by polymering monomer A, and then added B when most of A has reacted. In the isolated macroinitiator method, polyA which with halogen-terminated is isolated, and then polyA is used as a macroinitiator worked with CuX to polymerize monomer B. In this thesis, ATRP method is used to synthesize polymer. Polydispersity index is controllable in ATRP, and the final polymer could have functional group from the initiator chose.

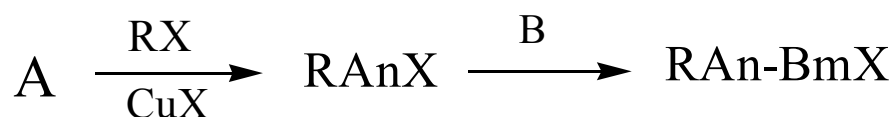


Figure 2. 22 Block copolymer mechanism of ATRP

2.6.2 Stable Free-Radical Polymerization (SFRP)

Stable free-radical polymerization used nitroxide, triazoliny, dithiocarbamate, and tritly as the mediation or persistent radical. Cyclic nitroxide radical: 2,2,6,6-tetramethyl-1-piperidinoxyl (TEMPO) have been extensively studied [51]. Figure 2.23 shows the thermal decomposition of an alkoxyamine “2,2,6,6-tetramethyl-1-(1-phenylethoxy)piperidine” into a reactive radical and a stable radical. Nitroxide radical which have steric hindrance were sufficiently stable.

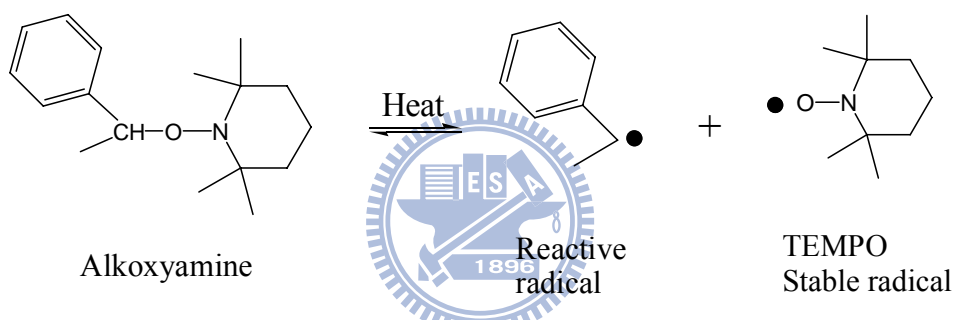


Figure 2. 23 the thermal decomposition of an alkoxyamine into a reactive radical and a stable radical

SERP process is analogous to ATRP as shown in Figure 2.24. The reactive radical initiate polymerization with the stable nitroxide radical, and the stable nitroxide radical mediate the reaction by reacting with propagating radicals to lower concentration. The nitroxide radical may not react with itself, and the nitroxide radical reacte rapidly with the propagation radical to decrease the concentration of the propagation radical. In SERP, the conventional bimolecular termination is negligible.

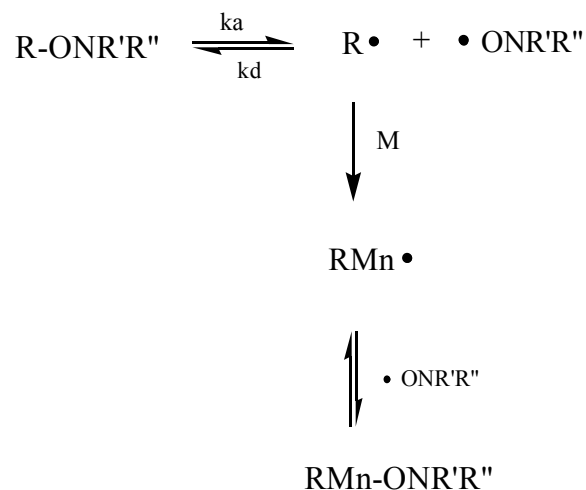


Figure 2. 24 Mechanism of SERP

2.6.3 Radical Addition-Fragmentation Transfer (RAFT)

Radical addition-fragmentation transfer living polymerizations controlled chain growth through reversible chain transfer [52]. A chain-transfer agent transferred a labile end group to a propagating chain as shown in Figure 2.25. The transfer reaction in RAFT is not a one-step transfer of the labile end group, but involve radical addition to the thiocarbonyl group of the dithioester. A new dithioester and new radical are form after the reaction ended.

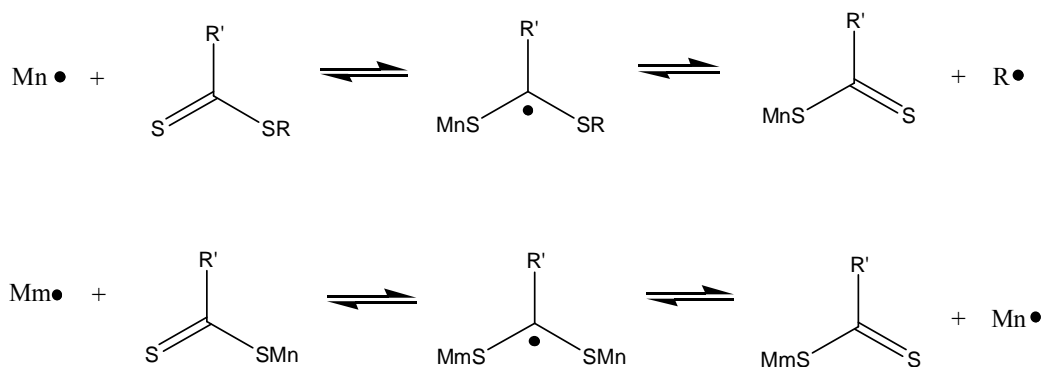


Figure 2. 25 Mechanism of RAFT

2.7 Cross-linking of siloxane

There are four classes siloxanes cross-linking reactions: (1) peroxide-induced free radical reaction, (2) condensation reactions, (3) hydrosilylation addition reactions, and (4) hydridosilane/silanol reaction. In this thesis, we focus on the condensation reactions as shown in Figure 2.26. Silicon would react with water to produce silanol groups, and silanol groups would further react with the starting materials or another silanol group to produce a siloxane cross-link.

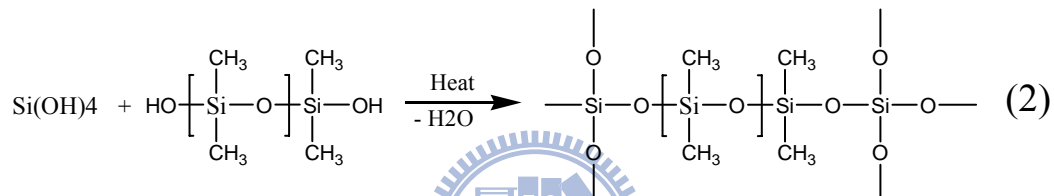
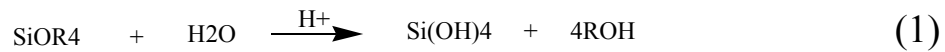


Figure 2. 26 Condensation reaction in the siloxane cross-linking

Figure 2.27 shows methyltrimethyl silane (MTMS) was sol-gel to methylsilsesquoxane (MSQ). After the sol-gel reaction was ended, MSQ would cross link to form a polymer. The final result was polytrimethylsiloxane with cage and network structures. The MSQ has good oxidative resistance, good thermal stability, and chemical stability.

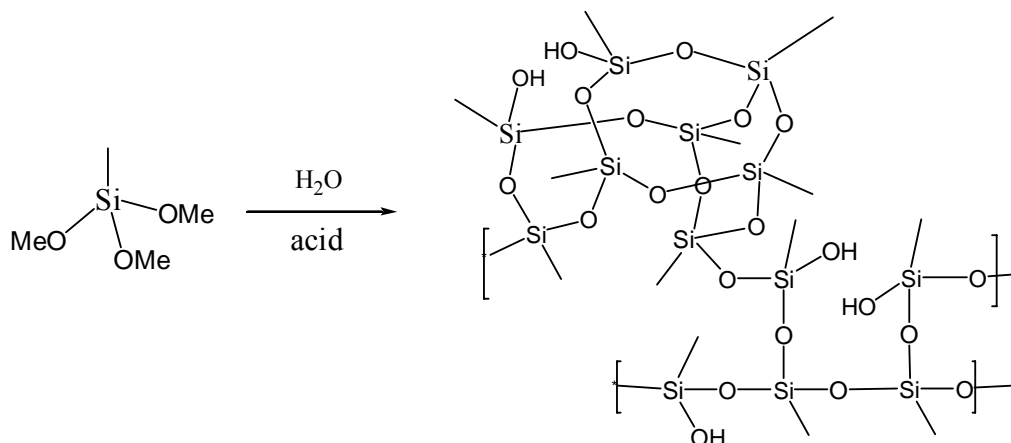


Figure 2. 27 Sol gel MTMS to MSQ

2.8 Characterization Methodologies

2.8.1 Nuclear Magnetic Resonance Spectroscopy (NMR)

The theory of NMR spectroscopy was proposed by W. Pauli in 1924. W. Pauli suggested that certain atomic nuclei should have the properties of spin and magnetic moment. In 1946, Bloch and Purcell demonstrated that nuclei absorb electromagnetic radiation in a strong magnetic field as a consequence of the energy level splitting that was induced by the magnetic field. Many atomic nuclei have a property called spin: the nuclei behave as if they were spinning. Spin angular momentum would show on odd mass, odd atomic number, or both have a quantized spin angular momentum and a magnetic moment. The more common nuclei that possess spin include: ${}^1_1\text{H}$, ${}^2_1\text{H}$, ${}^{13}_6\text{C}$, ${}^{14}_7\text{N}$, ${}^{17}_8\text{O}$, and ${}^{19}_9\text{F}$. A hydrogen nucleus may have a clockwise (+1/2) or counterclockwise (-1/2) spin, and the nuclear magnetic moment (μ) in the two cases are pointed in opposite directions. The nuclear magnetic resonance phenomenon occurs when nuclei aligned with an applied field are induced to absorb energy and change their spin orientation with respect to the applied field. Many nuclei are capable of exhibiting magnetic resonance; the organic chemist is interested in proton and

carbon resonances. Si for semiconductor related fields not all protons has resonance at the same frequency. The protons are shielded by the electrons that surround them. The resonance frequency would be controlled by shielded. A field-independent measure called the chemical shift (δ). From the different chemical shift, the organic compound structure can be demonstrated. The signal would through Fourier transform to become readable signal. Noise is random electronic signals that are usually visible as fluctuations of the baseline in the signal, and increase scan time would decrease noise signal. There were two general types of NMR spectrometers: (1) continuous-wave (CW) and pulsed, and (2) Fourier transform (FT NMR). In 1970, Ft NMR became the mainly NMR spectrometer.

2.8.2 Gel Permeation Chromatography (GPC)

GPC, also called size exclusion chromatography (SEC), the most widely used method of determining molecular weight distribution [53,54,55]. GPC column equips with a highly porous material with solvent to separate the polymer molecules size. Small molecules diffuse into the pores of the column more efficiently, hence small molecules travel through the column more slowly. Larger molecules would travel out the column first. From the plot of detector response against time of polymer molecules going through the column could in ensue polymer molecular weight. Figure 2.28 shows the schematic diagram of GPC [56].

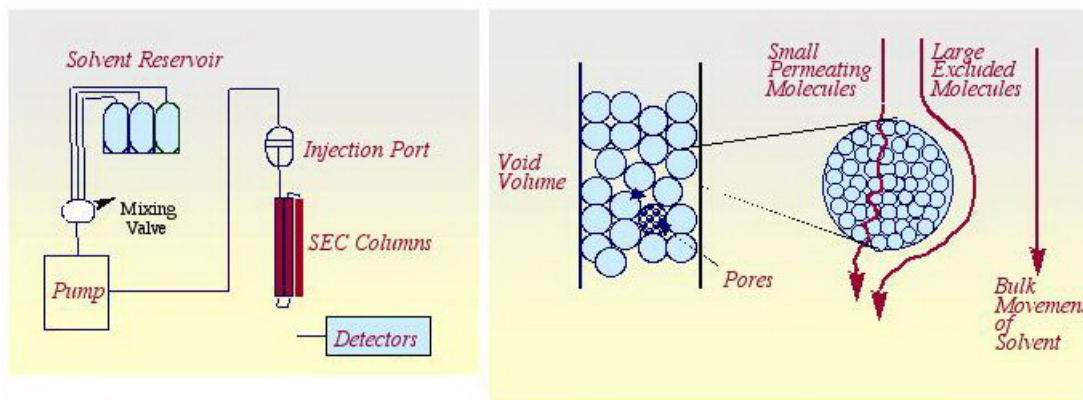


Figure 2. 28 Diagram of GPC

2.8.3 Different Scanning Calorimetry (DSC)

DSC is a thermal technique in which differences in heat flow into a substance and a reference are measured as a function of sample temperature while the two are subjected to a controlled temperature program. There were two types of DSC: (1) power compensated DSC, and (2) heat flux DSC. The instrumentation for the two was fundamentally different [57]. In this study, a heat flux DSC is used for measuring T_g .

Figure 2.29 shows the schematics of a heat flux DSC cell [58]. For heat flux DSC, heat flowed into both the sample and reference material via an electrically heated Constantan thermoelectric disk. The differential heat flow to two disks was monitored by Chromel/Constantan area thermocouples formed by the junction. The sample temperature was estimated by Chromel/Alumel junction under the sample disk.

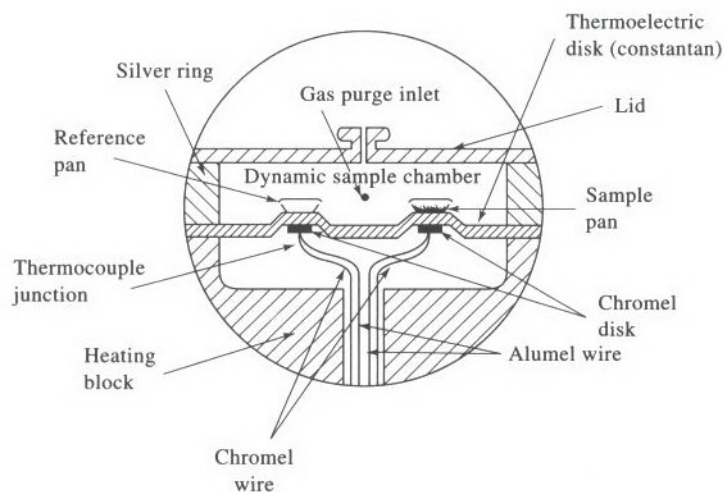


Figure 2. 29 Schematic of a heat flux DSC cell.

2.8.4 Thermal Gravimetric Analysis (TGA)

The mass of a sample in a controlled atmosphere is recorded as a function of temperature or time at fixed temperature. A plot of mass percent as a function of time is called a thermal decomposition curve. TGA instrument include: (1) a sensitive analytical balance, (2) a furnace, (3) a purge gas system for providing an inert atmosphere, and (4) a microcomputer/microprocessor for instrument control and data acquisition and display. Modern thermobalances used a computerized temperature control routine. The automatically compared the voltage output of the thermocouple with a voltage versus temperature table that was stored in read-only memory (ROM). The microcomputer used the difference between the temperature of the thermocouple and the temperature in ROM to adjust the voltage to the heater [59]. Typical run-to-run reproducibility fro a particular program fell within 2 °C throughout an instrument's entire operating range. Figure 2.30 shows the components of TGA [49].

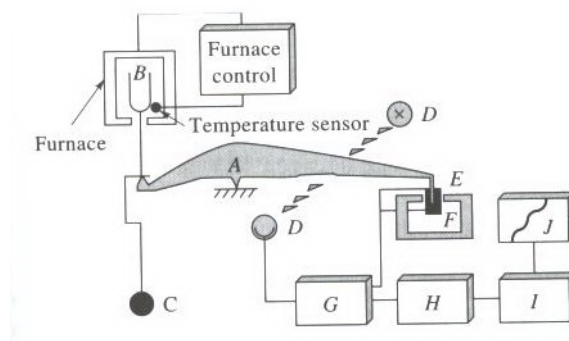


Figure 2. 30 Components of a thermal balance: A: beam, B: sample cup and holder, C: counterweight, D: lamp and photodiodes, E: coil, F: magnet, G: control amplifier, H: tare calculator, I: amplifier, J: recorder.

2.8.5 Fourier-transform infrared spectroscopy (FTIR)

A molecular was combined by atoms. Atoms had vibrational and rotational motion. For chemical purposes, “vibrational” portion of the infrared region was interested.

Hooke’s law [60] (Equation 2.4) shows the relationship between the frequency of the vibration, the masses of atoms and the bond strength.

$$\bar{\nu} = \frac{1}{2\pi c} \sqrt{\frac{k}{\frac{m_1 m_2}{m_1 + m_2}}} \quad (2.4)$$

where $\bar{\nu}$ = the vibrational “frequency” in cm^{-1}

c = the velocity of the light in cm/sec

k = the force constant of the bond in dynes/cm

m_1 = the mass of atom 1 in grams

m_2 = the mass of atom 2 in grams

Chemists prefer to use wavenumbers as unit, thus, the vibrational infrared extends from 4000 to 400 cm^{-1} .

FTIR has been applied to qualitative analysis, especially on organic compounds analysis. Pure silicon wafer which was as background, which would be first put on the FTIR holder, and nitrogen (N_2) was blow into FTIR. Infrared data is collected in the wavenumber from 4000 to 400 cm^{-1} using a total of 32 scans at 4 cm^{-1} resolution. Porous low-k film would be investigated on the same way.

2.8.6 Scanning Electron Microscope (SEM)

SEM images the sample surface by scanning it with high-energy electron source which is “Field emission source”. The detector gather secondary electrons signal, and transfer into an SEM photo through with amplifier. The sample has to coating metal layer (ex. Au, Pt) to alleviate charging effect.

In this study, SEM is Dual beam[focused ion beam & electron beam] system (FIB/SEM). The ion beam focused by electromagnetic lens to cut and etch in small dimension. Typical ion beam used liquid metal Gallium (Ga) ion source. The properties of ion source were low melting point, low vapor pressure and large resistance of oxidation. Equipments of FIB included liquid metal source, electromagnetic lens, second ion detector, scanning electrode, sample stage and vacuum system. Figure 2.31 shows schematic diagram of a FIB/SEM system.

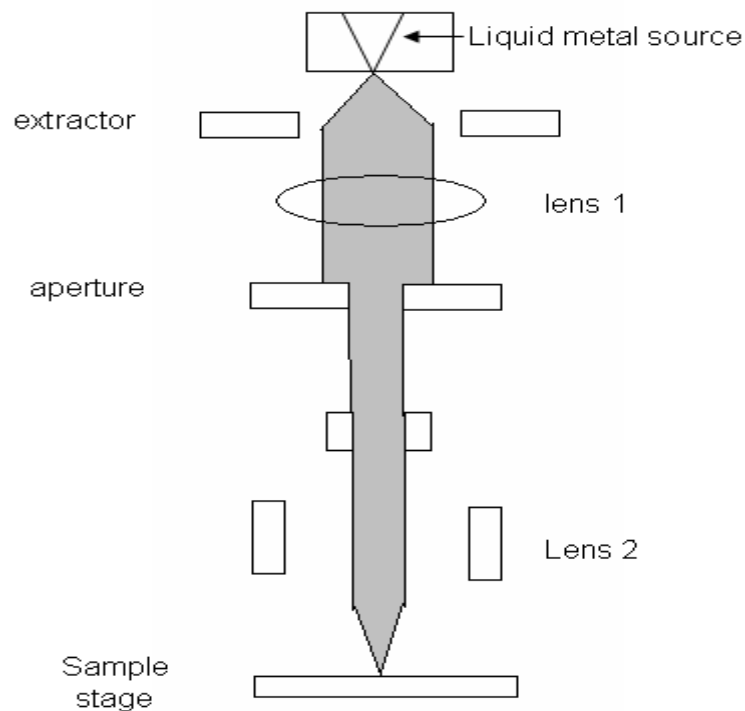
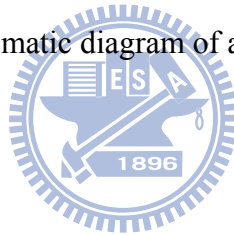


Figure 2. 31 Schematic diagram of a FIB/SEM system



2.8.7 X-ray reflectivity (XRR)

XRR is a non-contact surface analytical technique used in thin films, chemistry and material science. The source is copper $K\alpha$ ($\lambda=0.154$ nm), and the scan angle is from 0 to 2 degree. When the incident angle is very small (grazing incident angle), there has total reflection of X-ray from film surface. Beside, the reflection would decreased fast when the incident angle is larger then critical angle. In a rough surface, X-ray reflection would decrease faster than in a smooth surface. Therefore, there shows Kiiddig interference fringe in X-ray reflection curve when thin film was coated on the wafer. The frequency of would become larger when the difference between substrate and thin film get bigger. The period of Kiiddig interference fringe and thickness of thin film are opposite. More layers on the substrate and would have more

difference periods of Kiiddig interference fringe. Film thickness, film density and surface roughness could be investigated from Kiiddig interference fringe [61,62].

Figure 2.32 shows Kiiddig interference fringe of XRR.

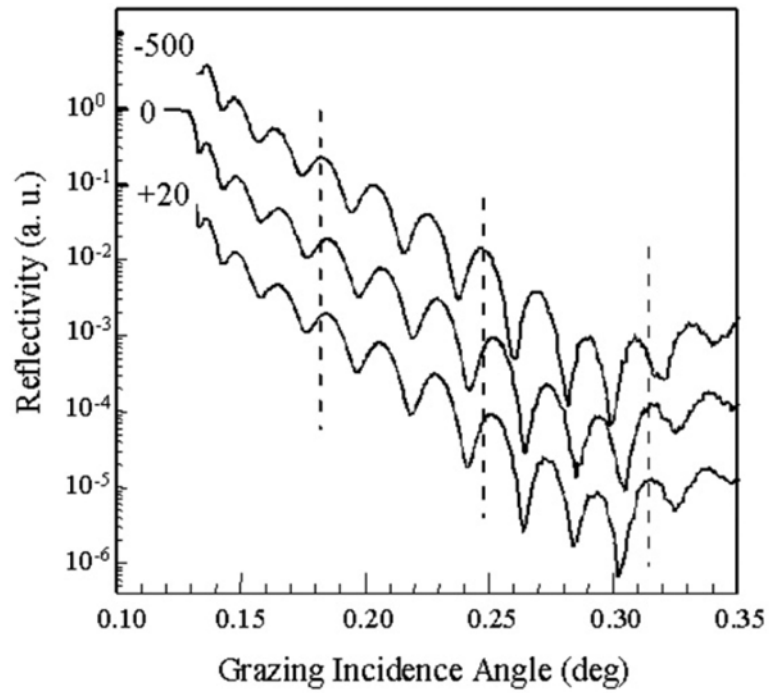


Figure 2. 32 Kiiddig interference fringe

Chapter 3 Experimental

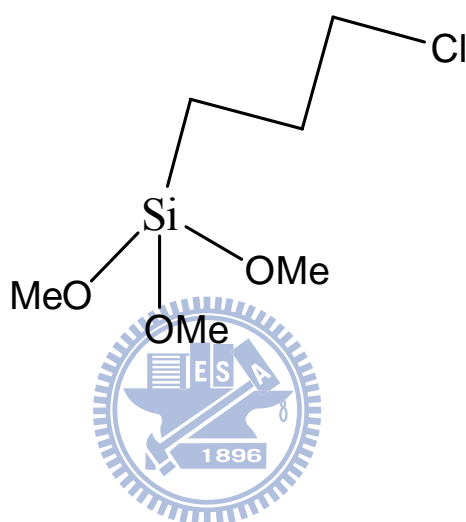
3.1 Materials

3.1.1 Chemicals

(1) Initiator

(3-chloropropyl)(triethoxy)silane

CAS No. 5089-70-3, purity=95%, product by TCI



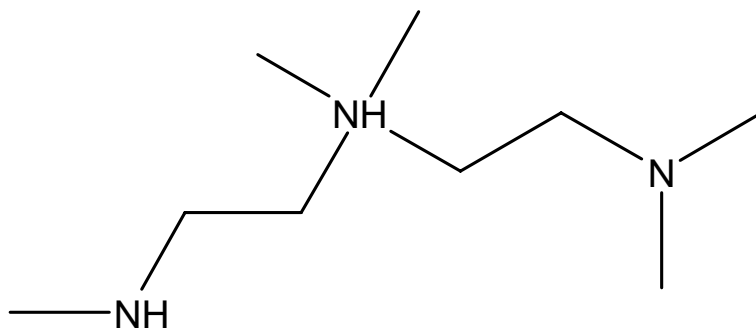
(2) Catalyst

(a) Copper (I) bromide

CuBr(I), CAS No. 7787-70-4, purity = 98%, product by Sterm Chemicals

(b) *N,N,N',N'',N'''*-pentamethyldiethylenetriamine

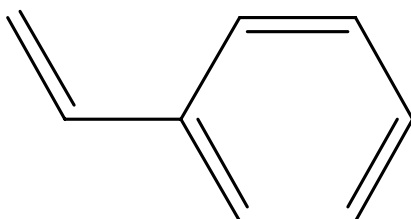
PMDETA, CAS No. 3030-47-5, purity = 99⁺%, product by ACROS



(3) Monomer

Styrene

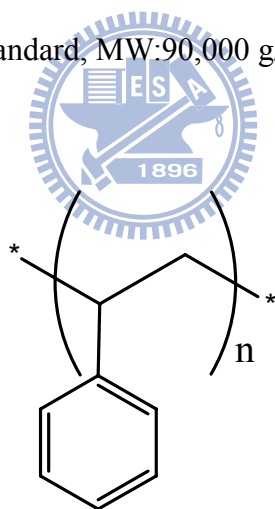
St, CAS No. 100-42-5, purity = 99%, product by SHOWA



(4) Polymer

Polystyrene

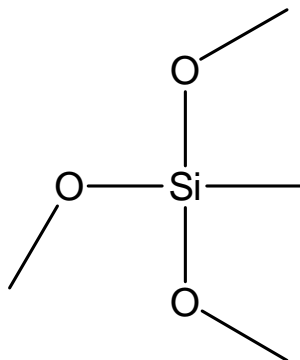
PS, CAS No.9003-53-6, standard, MW:90,000 g/mole, product by Aldrich



3.1.2 Matrix

methyltrimethoxysilane

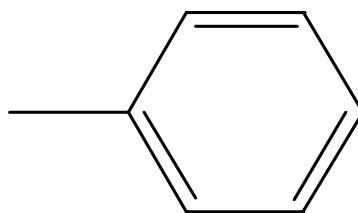
MTMS, CAS No. 1185-55-3, purity = 97%, product by ACROS



3.1.3 Solvent

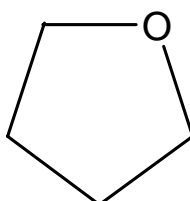
(1) Toluene

Toluene, CAS No.108-88-3, product by TEDIA



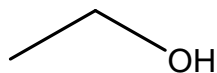
(2) Tetrahydrofuran

THF, CAS No. 109-99-9, purity =99.9, product by ECHO



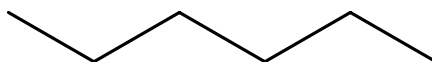
(3) Ethanol

EtOH, CAS No.64-17-5, purity =95, product by ECHO



(4) n-Hexane

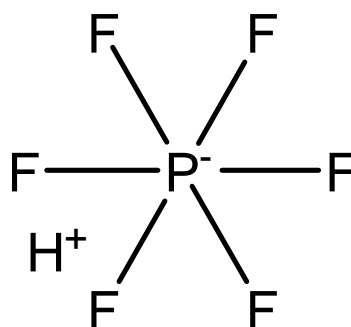
Hex, CAS No.110-545-3, purity >95 (HPLC), product by Aldrich



3.1.4 Acid

Hexafluorophosphoric acid

HPF6, CAS No. 16940-81-1, purity = 60wt%, product by ACROS



3.2 Preparation

3.2.1 Purification of styrene (St) and CuBr(I)

CuBr was sublimated before using. CuBr (20~30g) were added into a 250 mL flask with equipped magnetic stirring bar, and then added 1L acetic acid. The flask was wrapped by aluminum foil overnight. Acetic acid would be removed by methanol, and then removed methanol at 80 °C oven. The result was CuBr(I). Styrene was sublimated before using. Styrene was distilled to remove the inhibitor.

3.2.2 Synthesis of α -siloxane-polystyrene (PS-siloxane)

In this experiment, CuBr(I) (0.28g, 0.001 mole) was added to a 250mL flask, equipped with a magnetic stirring bar, and then the flask was degassed. Initiator SiCl (0.4g, 0.002 mole) was dissolved in 100 mL Toluene three freeze-pump-thaw cycles. Styrene (5.6g, 0.054 mole) was added in a 100 mL flask and degassed with three freeze-pump-thaw cycles. PMDETA (0.328g, 0.0002 mole) was transferred into the 250mL flask which carried CuBr(I) through a syringe, and CuBr(I) would dissolve in PMEDTA. PMEDTA was chosen as ligand to chelate CuBr(I), and activated CuBr(I). Toluene and initiator were transferred into the flask through a syringe. After 1 min, styrene was transferred into the flask through a syringe and stirred at 80 °C for 12 h under nitrogen atmosphere. The polymerization would be stopped by adding THF and Cu²⁺ was removed by an alumina column. The polymer (polystyrene-siloxane, PS-Siloxane) was obtained by precipitating the solution into alcohol and dried in the vacuum overnight. Yield: 1.3g (58.6%).

In this study, the ratio of styrene and initiator would be adjusted to change PS molecular weight. Table 3.1 shows the recipe of ATRP reactions for various PS molecular weight .

Table 3. 1 The recipe of ATRP reaction for various PS molecular weight.

	styrene	[I]	CuBr	PMDETA	Toluene	Time
(1)	5.6	0.4	0.28	0.328	3ml	12 h
(2)	5.6	1.2	0.28	0.328	3ml	12 h
(3)	5.6	2.4	0.28	0.328	3ml	12 h

3.2.3 Synthesis of MSQ from MTMS using sol-gel

MTMS (3.3g, 0.024 mole) was added into an alumina pan, DI water (0.285g, 0.018 mole) was added to hydrolysis MTMS, and added HPF_6 (0.0375g, 0.0003 mole) to dehydrate MTMS and start the sol-gel reaction. The pan was put into the oven at 80 °C for 7.5 mins to yield the final product, MSQ.

3.2.4 Grafting PS onto MSQ through siloxane-PS

Siloxane-PS was first dissolved in 2 mL THF in a 100 ml flask. Upon the completion of the sol-gel reaction, MSQ (1g) was immediately added into the flask. The reaction proceeded at 50 °C under oil bath for 14 h. The product was MSQ-g-PS, which was stored in freezer prior to usage.

3.2.5 Preparation of porous low-k film

MSQ-g-PS was dissolved in THF to form a 20 wt% solution. Before spin coating, the solution was initially filtered through a 0.45 μm PTFE filter (Millipore Inc.) in another bottle. The MSQ-g-PS solution was spin coating onto a silicon wafer to obtain the desired film thickness. The MSQ-g-PS film was then cured on a hot plate preheated at 200 °C for 30 mins, and at 400°C for 60 mins.

3.2.6 Solvent effect on the pore size of porous low-k films

Co-solvents such as ethanol/THF, hexane/THF at 5:1 ratio were employed in this

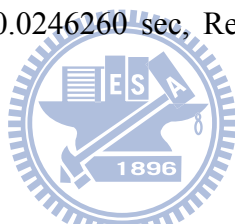
study to compare the PS sizes to that in pure THF solvent. Typically, THF was first added to dissolve MSQ-g-PS. Then ethanol or hexane was added to the MSQ-g-PS solution in order to examine coils size of PS long chain. Meanwhile, the thin film preparation method was the same as MSQ-g-PS porous low k film.

3.3 Experimental techniques

3.3.1 Nuclear Magnetic Resonance Spectroscopy (NMR)

^1H -NMR was employed to study the chemical structure of PS-Siloxane using Varian Unity-300 NMR. Chemical compound was dissolved in CDCl_3 . The relative sensitivity was 1.00 ppm, and the sample was scanned for 32 times.

^{29}Si -NMR was employed to study the chemical structure of using Bruker DSX-400WB NMR. Time was 0.0246260 sec, Repetition was 4096 times. Sample was solid.



3.3.2 Gel Permeation Chromatography (GPC)

GPC was employed to calculate the molecular weight of PS-Siloxane using GPC Water 1515, and sample was dissolved in THF. The ratio of sample/THF was 2mg/1mL. Flow was 1 mL/min at 45 °C.

3.3.3 Different Scanning Calorimetry (DSC)

DSC was employed to study the glass transition temperature of PS-Siloxane, which was produced by Perkin-Elmer. Sample weight must higher than 2 mg. The heating rate is 10 °C/min from 0 °C to 250 °C in nitrogen.

3.3.4 Thermal Gravimetric Analyses (TGA)

TGA was employed to study the decomposition temperature of PS-Siloxane and

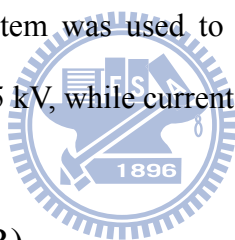
MSQ-g-PS using TA Q500. Sample weight must higher than 5 mg. The heating rate is 10 °C/min from 0 °C to 900 °C in nitrogen.

3.3.5 Fourier-transform infrared spectroscopy (FTIR)

Fourier-transform infrared spectroscopy (FTIR) was employed to study chemical structures of PS-Siloxane, MSQ, and MSQ-g-PS using MAGNA-IR Technology Protage 460 (Nicolet Inc.) from 400 to 4000 cm^{-1} . A transmission mode is typically used for porous low-k films onto a silicon wafer, which is infrared transparent. The total number of scans was 32 and the resolution was 4 cm^{-1} .

3.3.6 Scanning Electron Microscope (SEM)

A dual beam FIB/SEM system was used to examine the pore size of porous low-k films. Voltage was kept at 5 kV, while current was 98 pA.



3.3.7 X-ray reflectivity (XRR)

XRR was employed to characterize the porosity of porous low-k films using Beamline 13A1 in NSRRC, Taiwan. The scanning angle ranged from 0° to 2°, while the resolution was at 0.002°.

Chapter 4 Results and Discussion

There were three major topics in this chapter: (1) Synthesis and characterization of PS-siloxane, MSQ, and MSQ-g-PS, (2) Structure properties of MSQ-g-PS porous low k film such as pore size, morphology, porosity, and solvent effect for pore size, and (3) The comparison between PS/MSQ hybrid film and MSQ-g-PS film.

4.1 Synthesis and properties of PS-siloxane

4.1.1 Synthesis of PS-siloxane

Styrene monomer was polymerized to siloxane-polystyrene by ATRP method using (3-chloropropyl)(triethoxy)silane as an initiator as shown in Figure 4.1. The structure of PS-siloxane was validated by $^1\text{H-NMR}$ spectrum as shown in Figure 4.2.

Typically, PS has two major chemical structures: long chain and aromatic ring [63], while PS-Siloxane has additional siloxane as the end group. Therefore, there were three peaks of PS-Siloxane in $^1\text{H-NMR}$ spectrum: $\delta=1.25-1.84$ ppm (PS long chain), $\delta=6.45-7.18$ ppm (aromatic ring), and $\delta=3.6$ ppm ($-\text{OC}_2\text{H}_5$ of siloxane). The region of PS long train signal was separated to two portions: a: $\delta=1.25-1.54$ ppm, and b: $\delta=1.61-1.84$ ppm. “b” has higher chemical shift than “a” because of the electronegativity effect [64] on aromatic. Aromatic ring also has two peaks: c: $\delta=6.45-6.90$ ppm, and d: $\delta=7.03-7.18$ ppm because the aromatic ring current [65] made aromatic π -electron deshield aromatic protons, and caused peak separating. The content of siloxane was too low to affect the chemical shift of PS long chain. Therefore, PS-siloxane has almost the same $^1\text{H-NMR}$ spectrum as typical PS. The only difference is the distinctive siloxane signal ($\delta=3.6$ ppm) in PS-Siloxane. ATRP method can control radical stably, thus, PS-Siloxane was synthesized one by one from

styrene monomer. Siloxane initiator was the only radical source to start the polymerization and synthesized PS-Siloxane. Once signals of typical PS were shown in $^1\text{H-NMR}$ spectrum, the chemical structure was PS-Siloxane definitely.

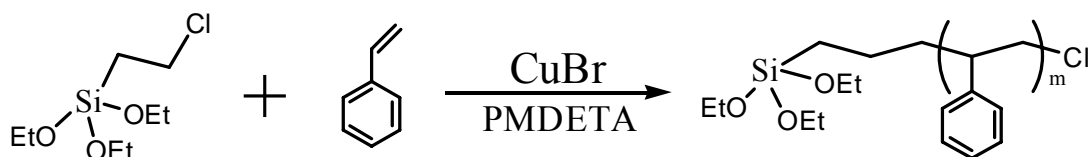


Figure 4. 1 Synthesis scheme of siloxane-polystyrene

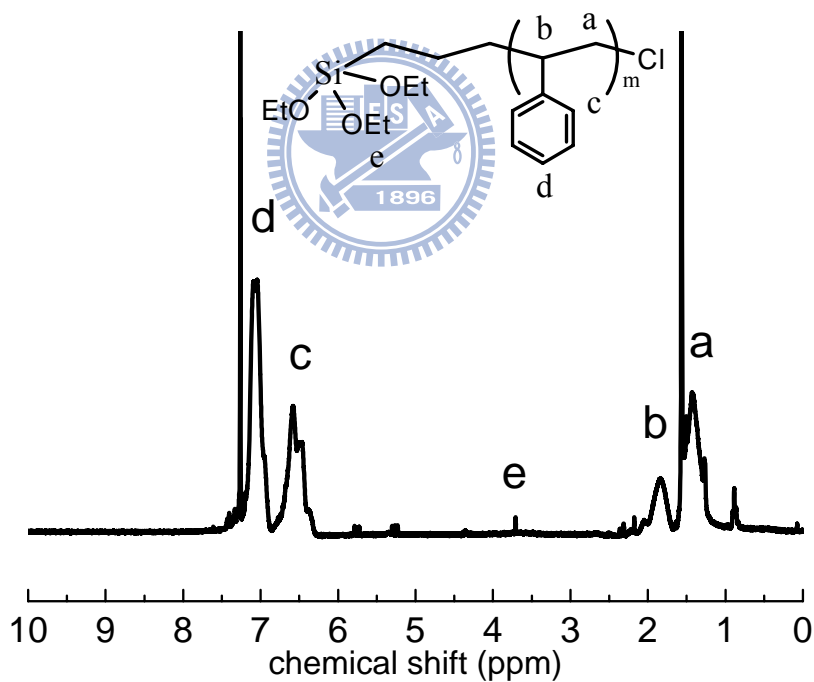


Figure 4. 2 $^1\text{H-NMR}$ spectrum of siloxane-PS

In order to obtain different pore sizes in the porous MSQ low-k films, it is critical to design the molecular weight of the grafted polystyrene porogens. Our

approach is to vary the amount of initiators in the ATRP synthesis of PS-Siloxane. Figure 4.3 showed the relationship between PS molecular weight and the content of initiator based on GPC measurement. PS molecular weight decreased from 80,000 to 5,000, when initiator weight loading increased from 0.4 g to 2.4 g. The relationship between initiator concentration and polymer molecular in ATRP method can be described by Equation 4.1 [66]. The molecular weight of polymer using ATRP synthesis was inversely proportional to both initiator and Cu^+ concentrations. It is believed that the numbers of radical were increased when the concentration of initiator or activator was increased [67]. When the content of radical was increased, the reaction can act faster, and styrene has no time to be polymerized. Therefore, PS molecular weight was decreased when the content of initiator was increased.

The molecular weight distribution of PS-Siloxane, such as polydispersity index (PDI) could be obtained from GPC data using Equation 4.2. For commercial polymer, the difference between M_w and M_n ($M_w > M_n$) or PDI increases as the molecular-weight distribution broadens [68]. When PDI value is close to 1, M_w value and M_n value were very close, *i.e.* a very narrow molecular weight distribution.

PDI values of PS with $M_n = 5000$ g/mole, 100,000 g/mole, and 80,000 g/mole were 1.38, 1.20, and 1.33, respectively, which were relatively low. In general, free radical polymerization would have PDI about 4 [69]. Low PDI value (~ 1.3) in this study was one of characteristic features of ATRP synthesis method.

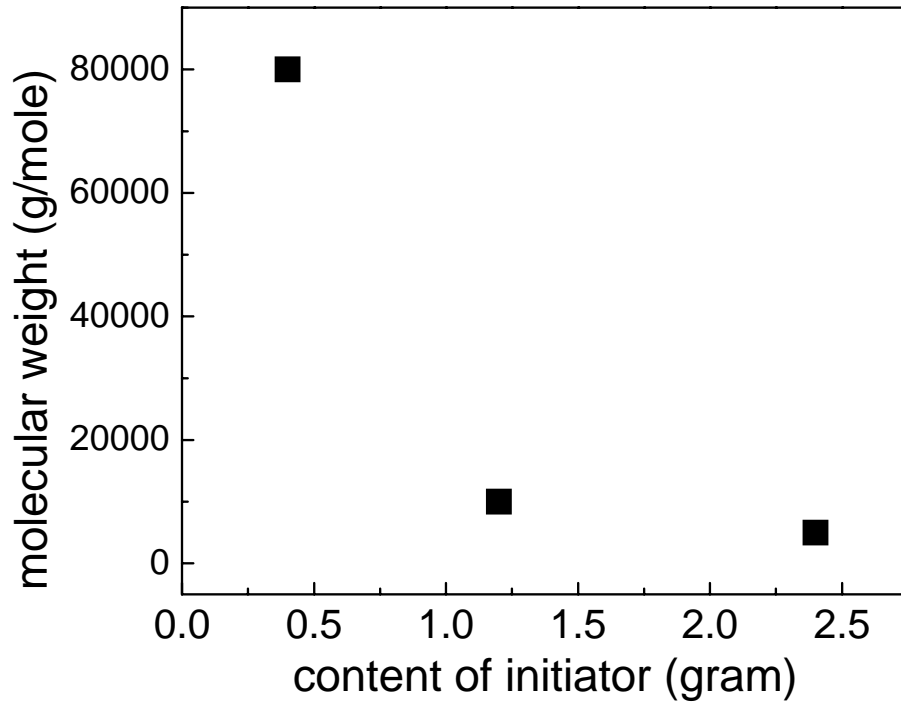


Figure 4. 3 PS molecular weight as a function of initiator weight loading

$$\ln \frac{[M]_0}{[M]} = \frac{3k_p}{2} \left\{ \frac{K[I]_0[Cu^+]_0}{3k_t} \right\}^{1/3} t^{2/3} \quad (4.1)$$

Where

$[M]_0$ = initial concentration of monomer

$[I]_0$ = initial concentration of initiator

$[M]$ = monomer concentration

$[Cu^+]$ = Cu^+ concentration

$K = k_a/k_d$,

k_a = rate constant for activation

k_d = rate constant for deactivation

t = time

$$\text{PDI} = M_w/M_n \quad (4.2)$$

M_w = weight average molecular weight

M_n = number average molecular weight

4.1.2 Thermal properties of PS-Siloxane

Next, the thermal properties such as thermal stability and glass transition temperature (T_g) of the functionalized porogen, PS-siloxane was investigated to realize its basic properties. Figure 4.4 shows the thermo-gravimetric curve of PS-siloxane from room temperature to 800 °C. The weight loss below 100 °C was believed to be caused by the loss of solvent (THF). The complete decomposition of PS-siloxane occurred at 435 °C. Moreover, T_d of PS-siloxane was 362 °C at which 5% weight loss occurred. Thus, the novel functionalized porogen, PS-siloxane possessed a high decomposition temperature, which was the primary requisite for high-temperature porogen in the Solid-First™ scheme. As a result, PS-siloxane is an excellent high-temperature porogen.

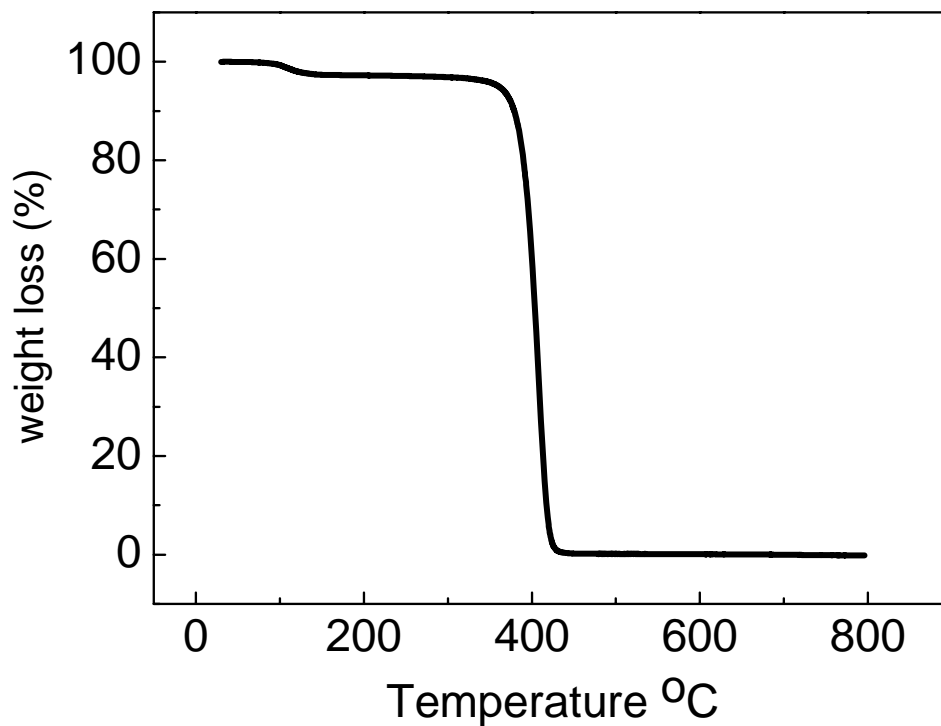
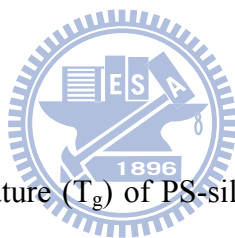


Figure 4. 4 TGA of PS-Siloxane



The glass transition temperature (T_g) of PS-siloxane was examined by scanning calorimetry (DSC) as shown in Figure 4.5. T_g can be defined from the thermal linear dimension change. T_g of PS-Siloxane was calculated at 122 °C based on the thermal linear dimension changed from 103 °C to 138 °C. T_g was measured to realize another property of PS-Siloxane.

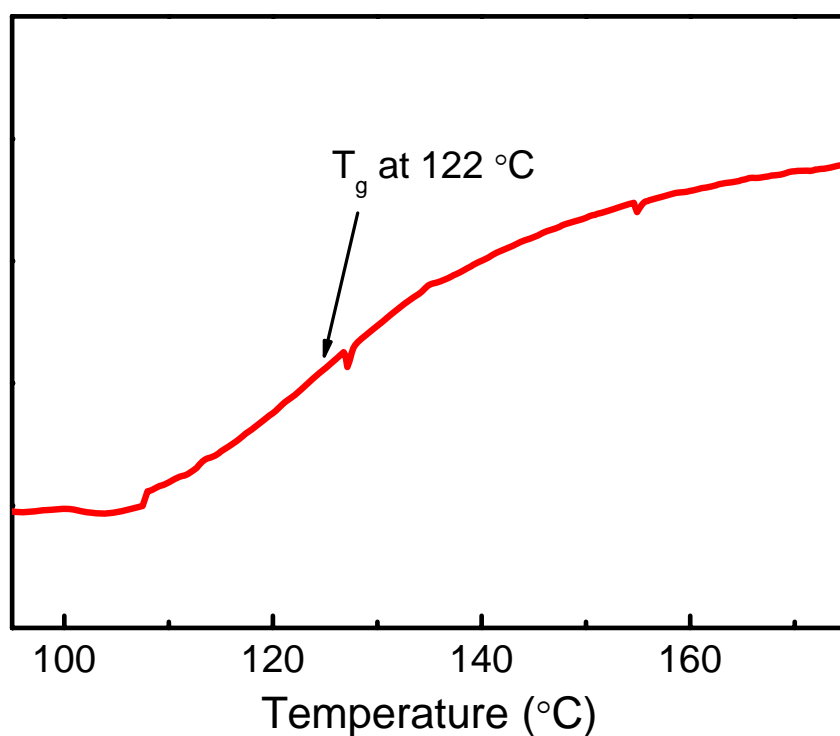
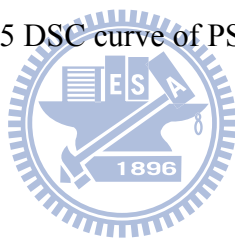


Figure 4.5 DSC curve of PS-siloxane



4.2 Synthesis of MSQ

MTMS monomers were polymerized to MSQ under acid condition by sol-gel method as illustrated in Figure 4.6, where “cage” and “network” Si-O were two major chemical structures of MSQ matrix. FT-IR spectroscopy was employed to examine the chemical bonding and structural change of MSQ cured at different temperatures: (a) 60 °C and (b) 400 °C, as shown in Figure 4.7. The primary infrared absorption peaks and their chemical bonding assignments were summarized in Table 4.1 [70]. The important absorption peaks were the Si-O-Si (cage like structure) peak at 1130 cm^{-1} , the Si-O-Si (network like structure) peak at 1023 cm^{-1} , the methyl (CH_3) stretching band at 2969 cm^{-1} , bending mode at 1275 cm^{-1} , Si-OH absorption peak at 911 cm^{-1} and Si-C absorption at 780 cm^{-1} .

When cure temperature was increased from 60 °C to 400 °C, cage structure was

destroyed and transformed into network structure as observed the increase of peak intensity at 1023 cm^{-1} from 60 to $400\text{ }^{\circ}\text{C}$.

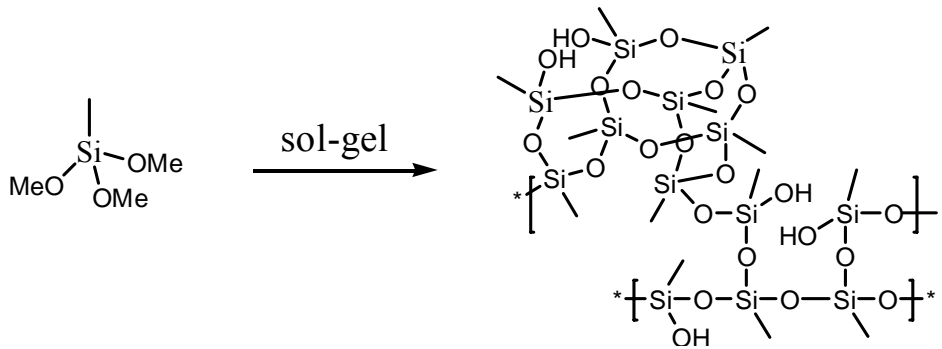


Figure 4. 6 The schematic of MSQ synthesis from MTMS monomers

Table 4. 1 Primary absorption peak position and their assignment

Wavenumber (cm^{-1})	Chemical Bonding
781	SiC-H ₃
911	Si-OH
1023	Si-O-Si (network)
1130	Si-O-Si (cage)
1275	-CH ₃ (bend)
2969	-CH ₃ (stretch)

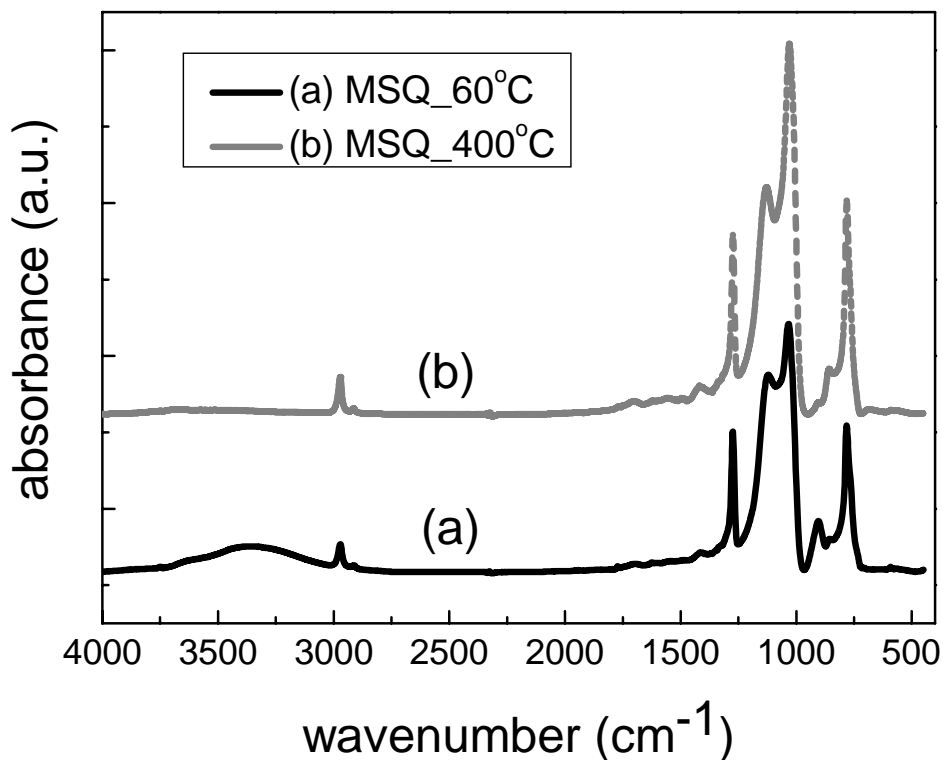


Figure 4. 7 FTIR spectra of MSQ cured at 60 °C and 400 °C



4.3 Grafting PS-siloxane onto MSQ

PS was grafted onto MSQ through the functional group, siloxane end-cap of PS-siloxane by sol-gel method as illustrated in Figure 4.8. In order to confirm whether PS has been grafted onto MSQ through functional siloxane end-group, thermal analysis of MSQ and MSQ-g-PS were carried out and compared as shown in Figure 4.9. For MSQ, H₂O groups escaped during the thermal process from 200 °C to 550 °C and caused weight loss. However, the decomposition curve of MSQ-g-PS showed not only the escaping H₂O, but also other weight loss which was considered to relate with PS loss. In order to analyze this weight loss in-depth, two curves in Figure 4.9 were transformed to their corresponding derivative curve as illustrated in Figure 4.10 and Figure 4.11, respectively. Figure 4.10 showed only slightly change from 200 °C to

550 °C in MSQ. However, there was obvious weight loss from 376 °C to 460 °C from the derivative curve of MSQ-g-PS in Figure 4.11. PS broke away from MSQ in this thermal range, and its thermal decomposition temperature, T_d in MSQ-g-PS was calculated as 383 °C. When PS was grafted onto MSQ through functional siloxane end-group, the rigid MSQ structure surrounding PS distributed the energy of breaking PS. Thus, the thermal property of PS was enhanced from 362 °C (pure PS) to 383 °C. Thermal decomposition data provide the other supporting evidence for the successful grafting of PS onto MSQ through PS-siloxane end-cap group.

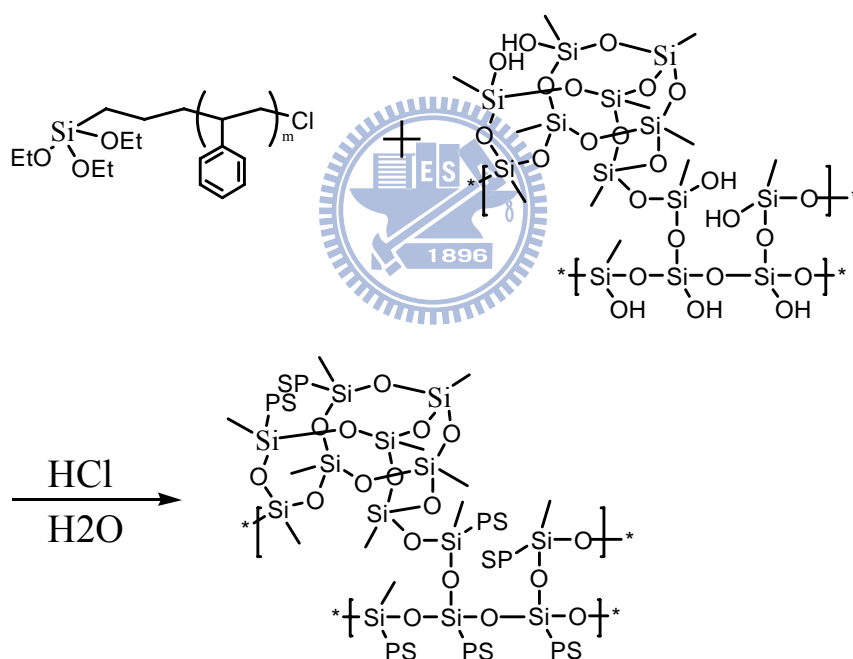


Figure 4. 8 Schematic reaction diagram of grafting PS onto MSQ through siloxane-PS

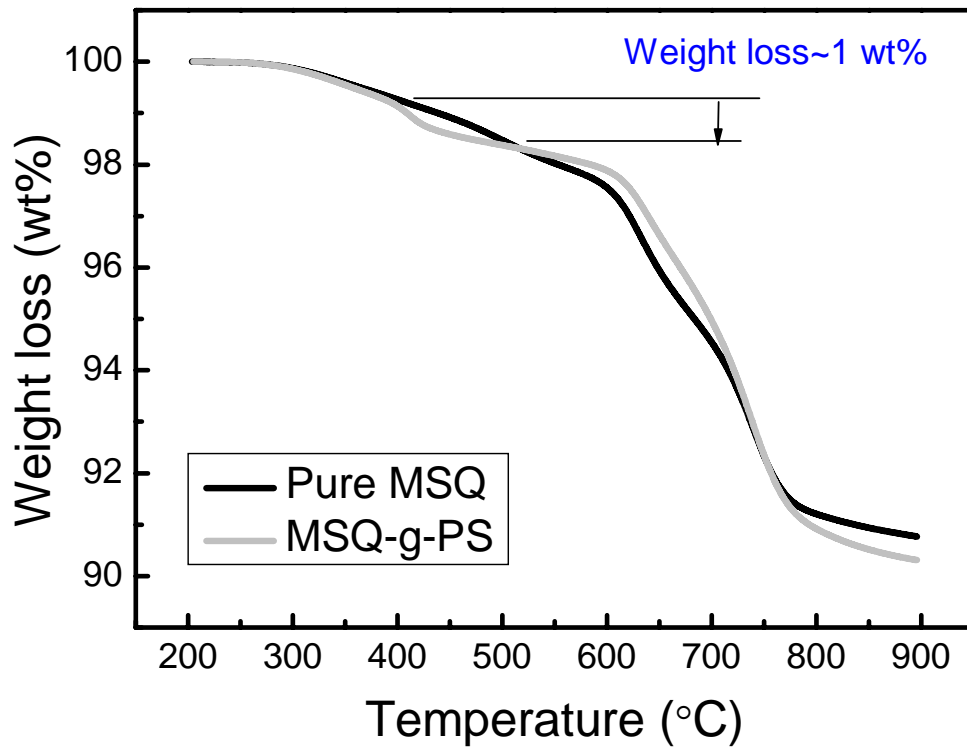


Figure 4.9 TGA data of MSQ and PMS-g-PS

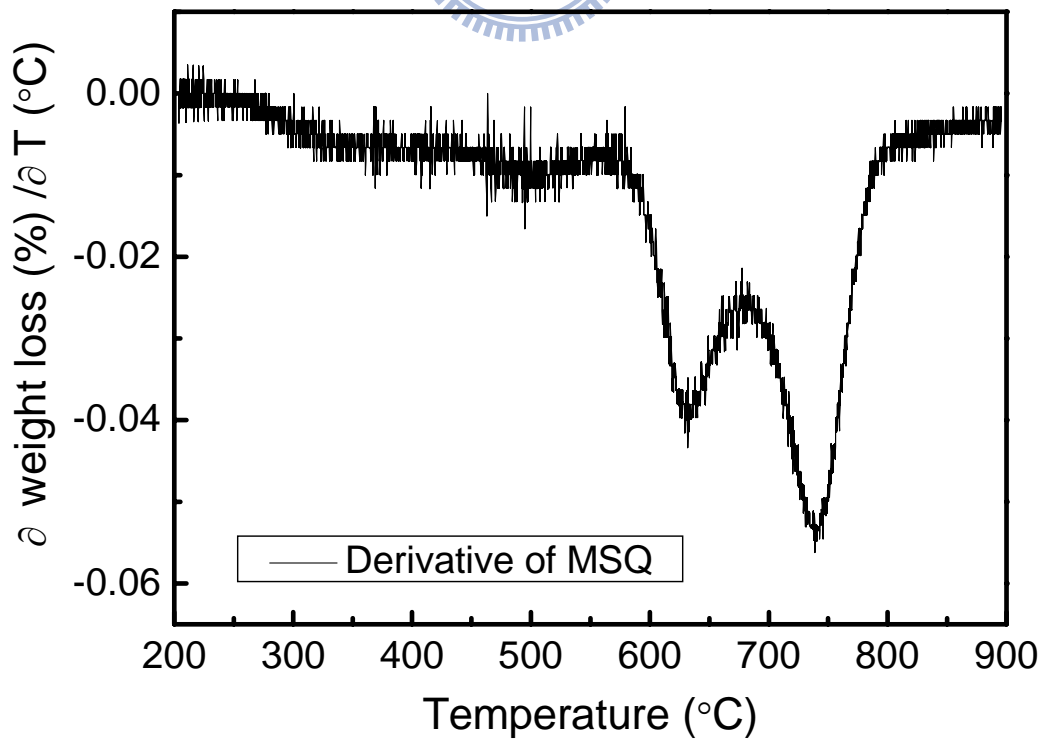
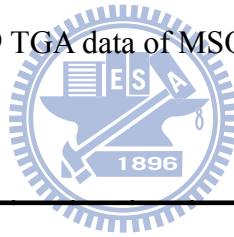


Figure 4.10 Derivative of TGA data of MSQ

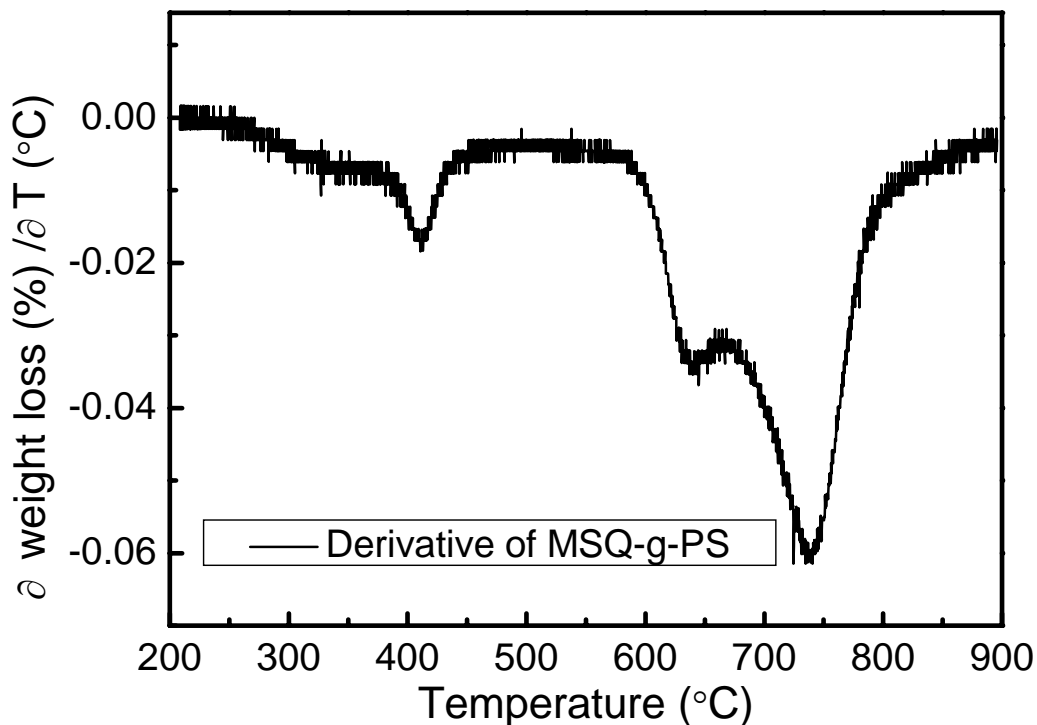


Figure 4.11 Derivative of TGA data of MSQ-g-PS



The changing of silane group was a evidence to demonstrate whether PS-Siloxane was grafted onto MSQ. This section would employ FTIR, TDS, and ^{29}Si -NMR to investigate silane group of MSQ-g-PS structure. Figure 4.12 shows IR spectra of MSQ-g-PS. PS signal did not show in FTIR spectra, because PS only have 1 wt% of MSQ and the resolution of FTIR was 5 wt%. Table 4.1 shows the peak assignment of IR spectra. Figure 4.13 shows TDA data of CH_4 escaped from MSQ. Figure 4.14 shows ^{29}Si -NMR spectra of MSQ and MSQ-g-PS structures. Table 4.2 summarizes the peak assignment of ^{29}Si -NMR spectra [71]. The mechanism of how PS-Siloxane is grafted onto MSQ will be discussed on next page.

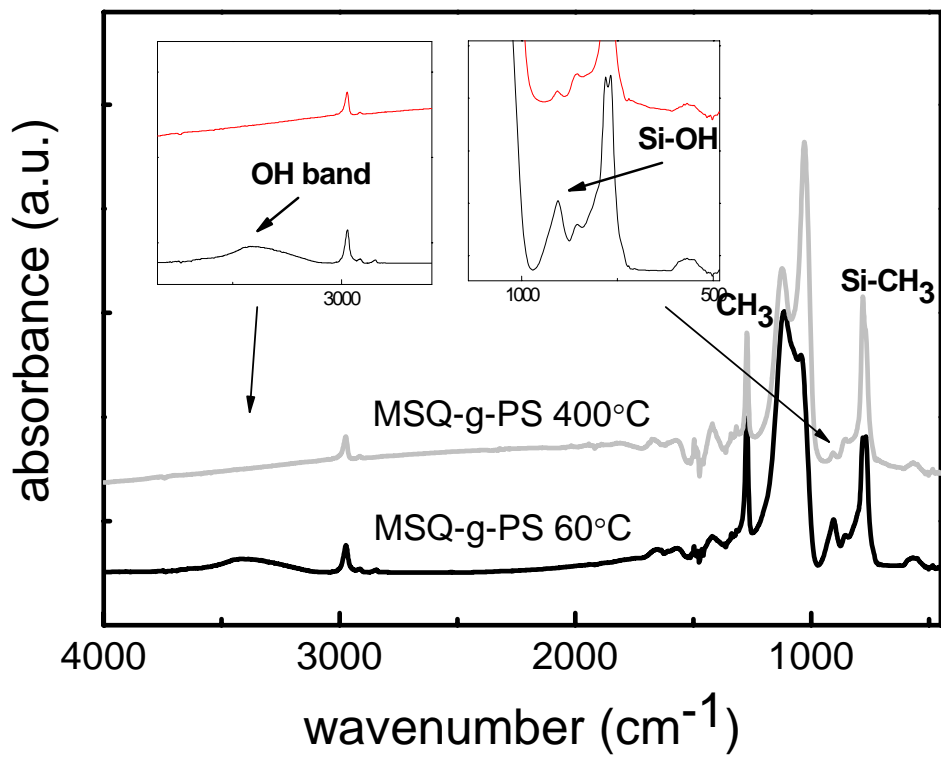


Figure 4. 12 IR spectra of MSQ-g-PS

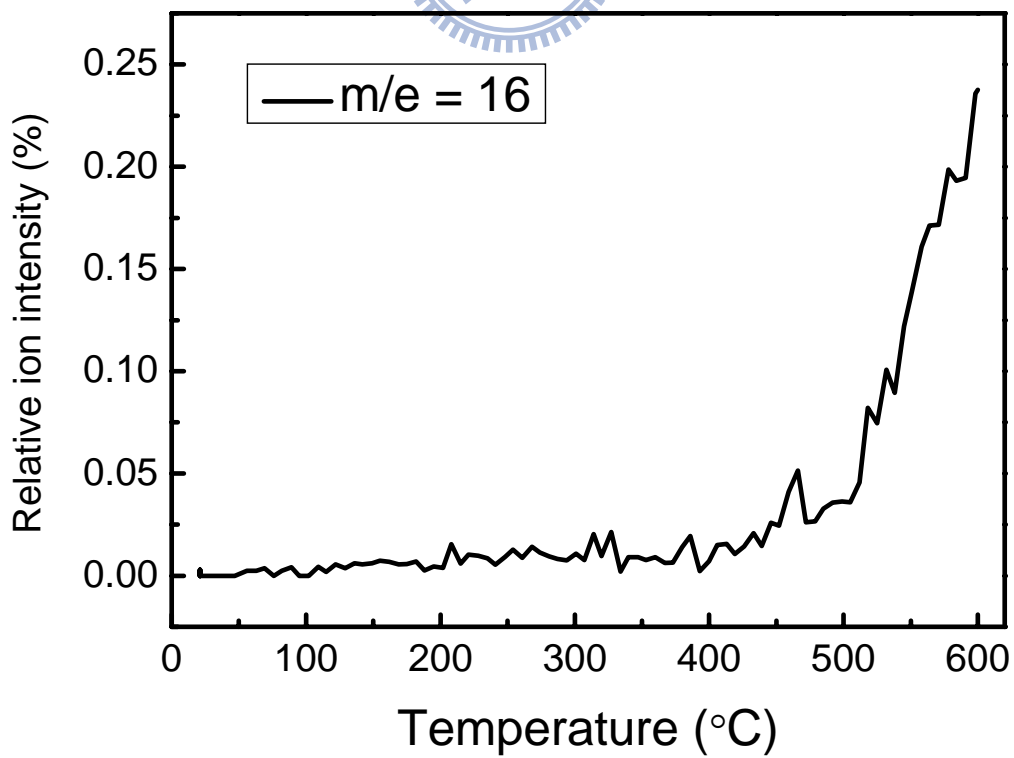


Figure 4. 13 TDS of CH_4 for where CH_4 evolution data of MSQ

Table 4. 2 peak assignment of ^{29}Si -NMR spectra

	Assignment	Position (ppm)
Q^4	$[(\text{SiO})_4\text{Si}]$	-119.1
Q^3	$[(\text{SiO})_3\text{Si}(\text{OH})]$	-102.1
	$[(\text{SiO})_3\text{Si}(\text{OMe})]$	
T^3	$[(\text{SiO})_3\text{Si}(\text{CH}_3)]$	-64 to -69
T^2	$[(\text{SiO})_3\text{Si}(\text{OH})(\text{CH}_3)]$	-54 to -61
	$[(\text{SiO})_3\text{Si}(\text{OCH}_3)(\text{CH}_3)]$	

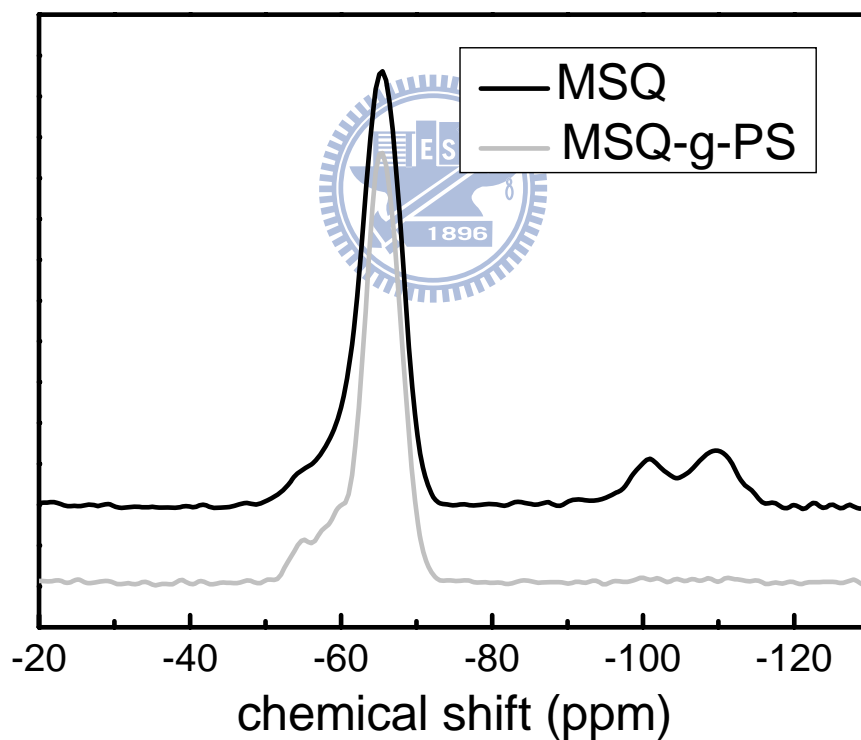


Figure 4. 14 ^{29}Si -NMR of MSQ-g-PS

From FTIR spectra, Si-CH₃ silane chemical bonding would not have huge decomposition in curing process. TDS shows that there has a little bit -CH₃ escaping from MSQ at 400 °C, and, huge -CH₃ escaping at 500 °C. The Si-CH₃ would break to Si- and -CH₃, and then Si- would combine with H₂O and another Si- become Si-O-Si. Moreover, -CH₃ would become CH₄ and leave. From ²⁹Si-NMR spectra, Q signal of MSQ was three MSQ siloxane structures and one Si-O-Si structure which was come from breaking Si-CH₃ chemical bond. Because there were no Si-OH signal in FTIR spectra, Q signal of MSQ in ²⁹Si-NMR spectrum does.

In order to comprehend how PS-Siloxane was grafted onto MSQ, 5 times PS were added into MSQ solution by sol-gel method. In the same curing condition with MSQ, when grafted PS onto MSQ, PS chain which has lower decomposition temperature would be burned out first and decreased the chance of Si-CH₃ broke. Therefore, there was no Q signal of MSQ-g-PS in ²⁹Si-NMR spectra. If PS did not graft onto MSQ, the ²⁹Si-NMR spectra would be the same as MSQ spectra. MSQ-g-PS structure can be demonstrated by ²⁹Si-NMR spectra.

4.4 Pore morphology of MSQ-g-PS porous low k film

The MSQ-g-PS porous low k film was prepared by spin coating, and then burned out PS porogen at 400 °C for 1 hour. This study produced two variables to control pore size, which were PS molecular weight and solubility of solvent. Pore size, pore morphology, and porosity would be discussed in this section.

4.4.1 The relationship between molecular weight and pore size in MSQ-g-PS

The relationship between PS molecular weight and pore size was examined by

Figure 4.15 through Figure 4.17. The average pore size were 160 nm, 100 nm, and 80 nm for PS M_w : 80,000g/mole, 10,000 g/mole, and 5,000 g/mole. Figure 4.18 summarized the pore morphology of MSQ-g-PS with various molecular weights. Pore size were plotted as a function of the square root of PS molecular weight as shown in Figure 4.19. When PS was core spherical in THF, the curve would be linear [72].

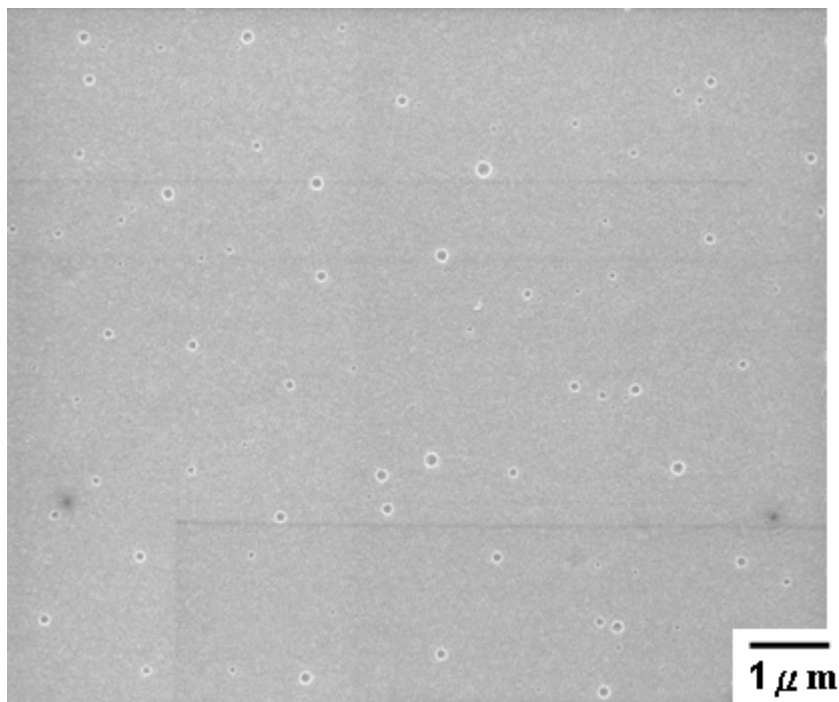


Figure 4. 15 SEM photograph of MSQ-g-PS porous low k film (MW of PS: 80,000 g/mole).

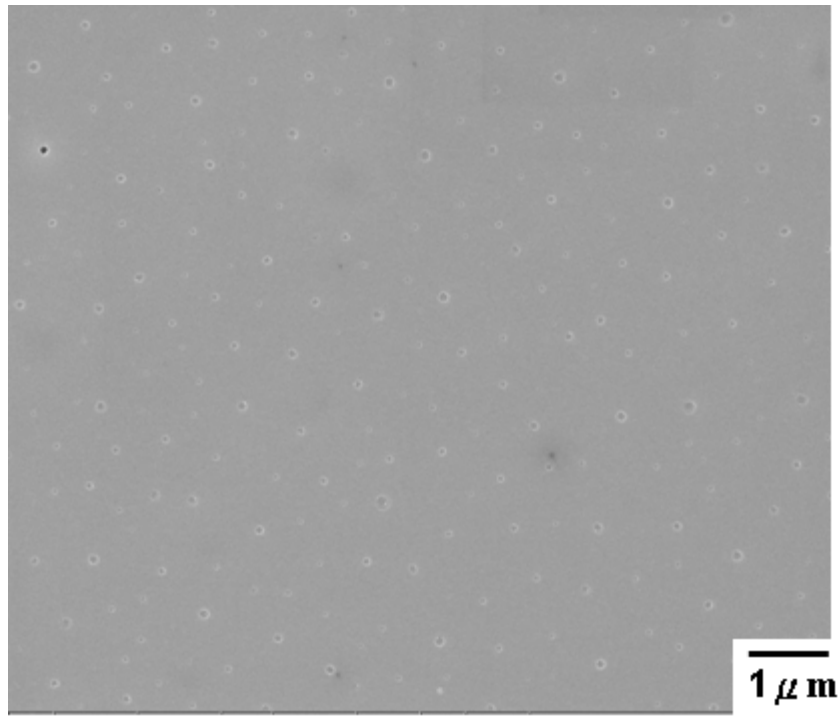


Figure 4. 16 SEM photograph of MSQ-g-PS porous low k film (MW of PS: 10,000 g/mole).

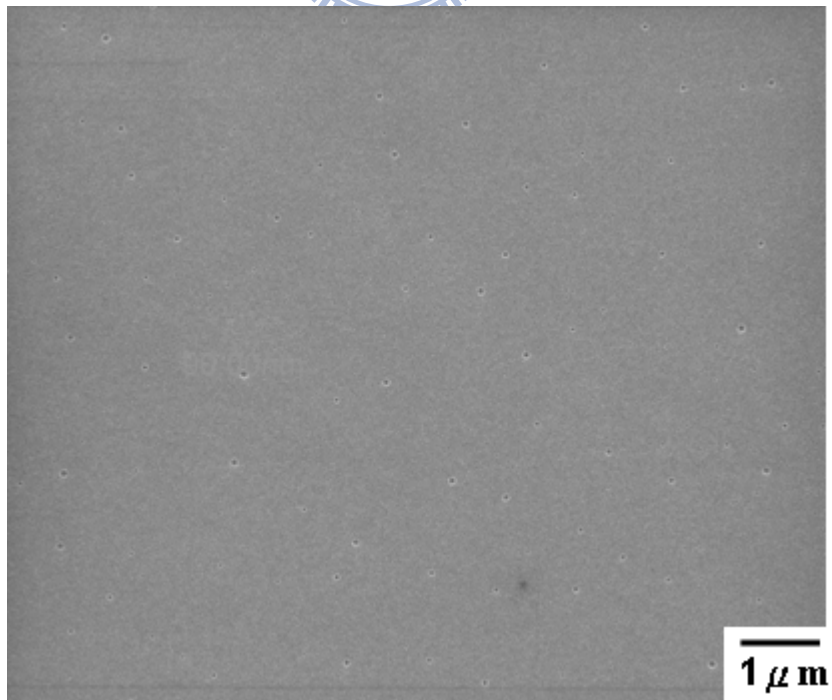
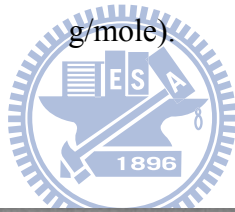


Figure 4. 17 SEM photograph of MSQ-g-PS porous low k film (MW of PS: 5,000 g/mole).

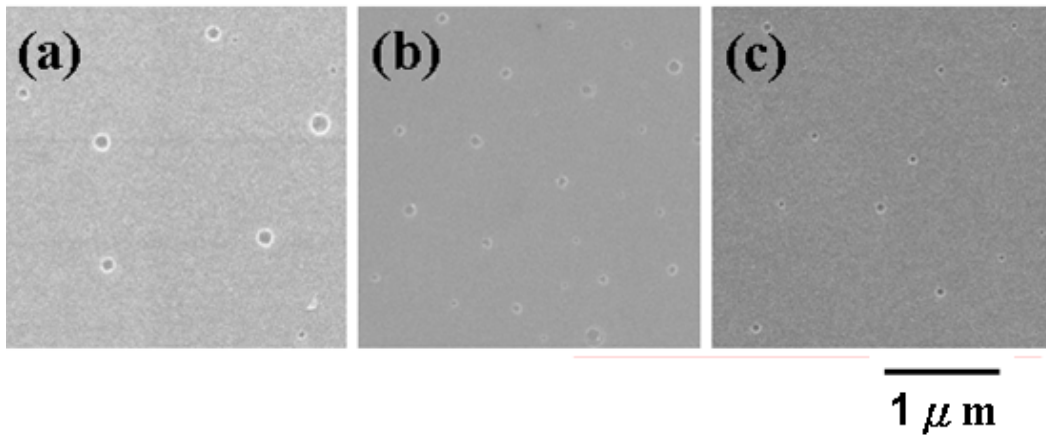


Figure 4.18 SEM of MSQ-g-PS low k films with various MWs: (a) 80,000 g/mole (b) 10,000 g/mole (c) 5,000 g/mole.

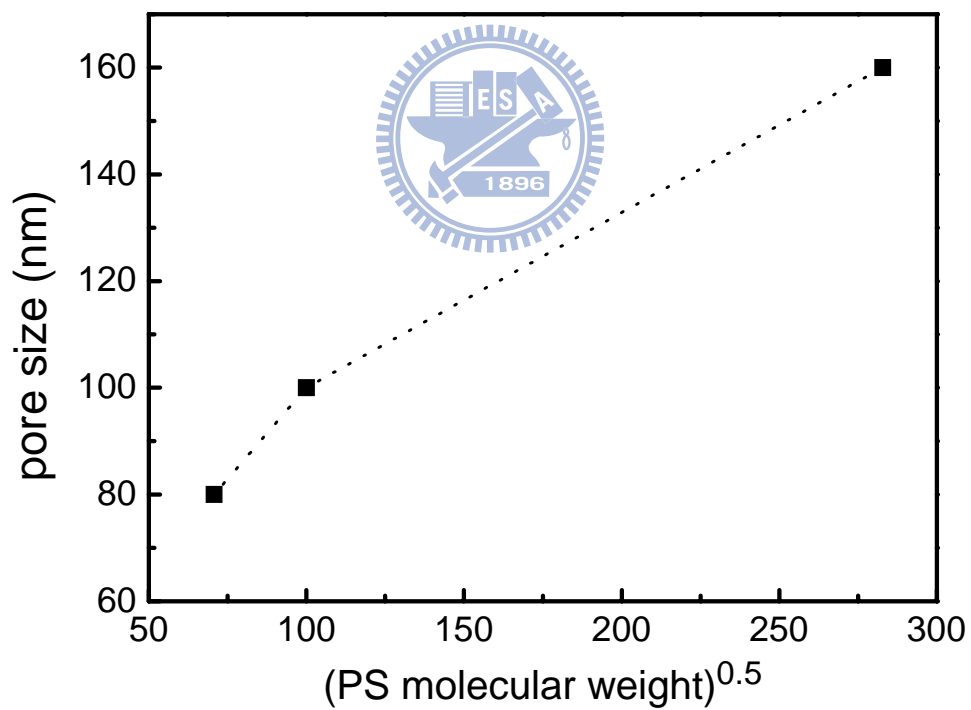


Figure 4.19 Pore size as a function of the square root of PS molecular weight

The equation of pore size and PS molecular weight can be expressed by Equation 4.3 [73]. From Equation 4.3, pore size and PS molecular weight were index movement. When PS molecular weight decreased, and the pore size would become smaller. In this study, diffusion parameter and polymer viscosity [74] were calculated, to be 10.24 and 0.24. Those parameters will be discussed in section 4.4.2.

$$R=a(M)^b \quad (4.3)$$

where

R= pore radius (nm)

M= polymer molecular weight (g/mole)

a= diffusion parameter

b= polymer viscosity



4.4.2 Solvent effect

The solvent effect on the pore size was further studied using co-solvents: ethanol/THF, hexane/THF, and THF. A THF-based co-solvent is chosen, because PS-Siloxane can not be dissolved in ethanol or hexane. Figure 4.20~25 show pore morphology of MSQ-g-PS film with PS molecular weight (80,000 g/mole, 10,000 g/mole, and 5,000 g/mole) and co-solvent (ethanol/THF and hexane/THF) as illustrated by SEM photograph. Figure 4.26 summarizes all of pore morphology photos in solvent effect and molecular weight studies. When co-solvent ethanol/THF or hexane/THF was added, pore size decreased.

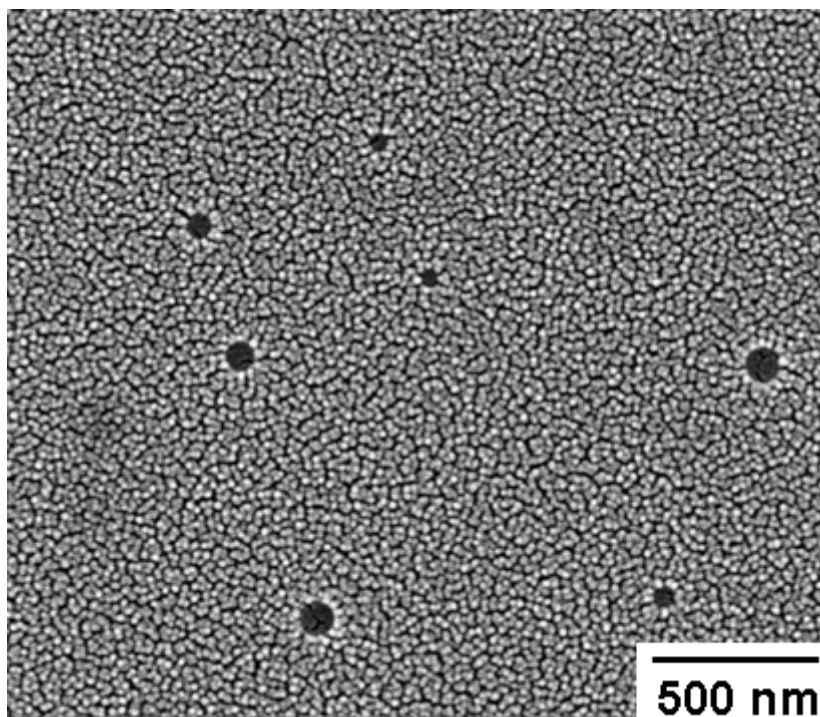


Figure 4. 20 PS M_w : 80,000 g/mole, solvent was Ethanol/THF

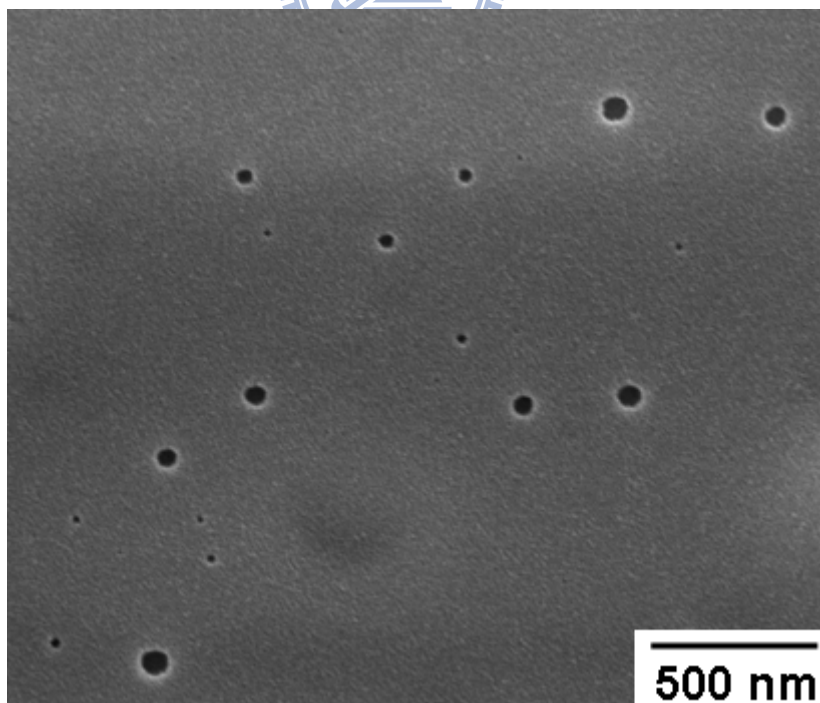


Figure 4. 21 PS M_w : 80,000 g/mole, solvent was n-Hexane/THF

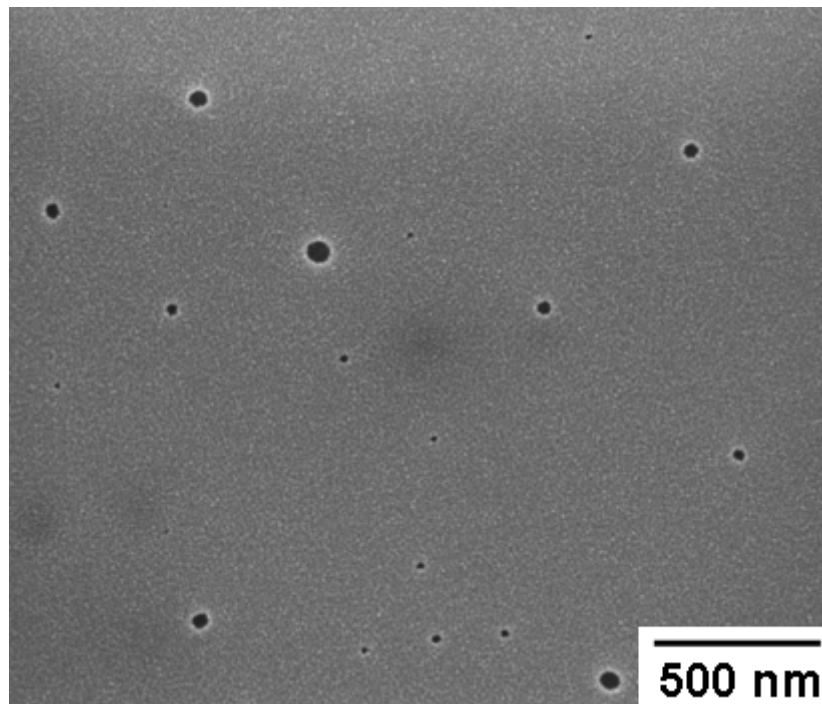


Figure 4. 22 PS M_w : 10,000 g/mole, solvent was Ethanol/THF

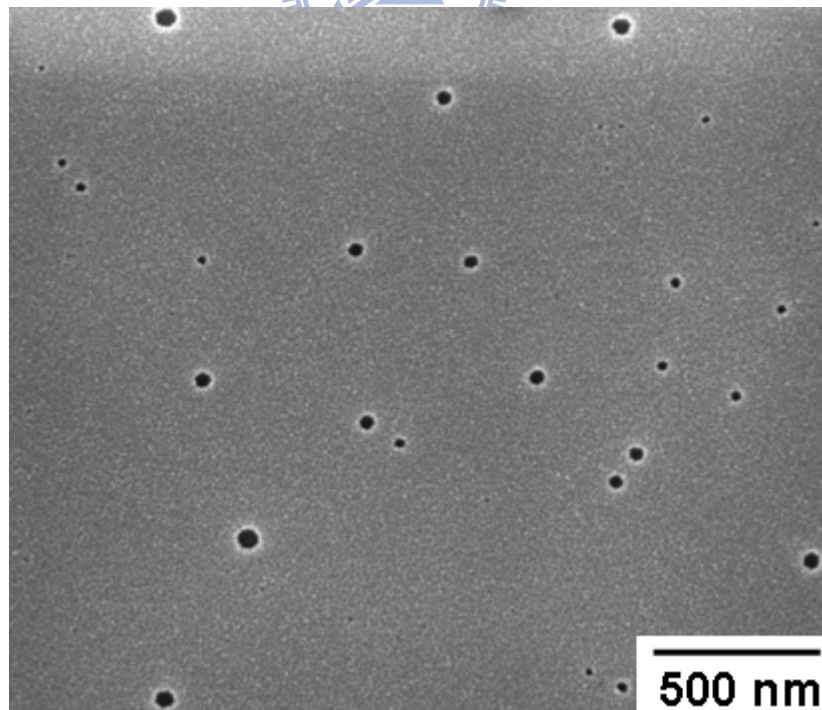


Figure 4. 23 PS M_w : 10,000 g/mole, solvent was n-Hexane/THF

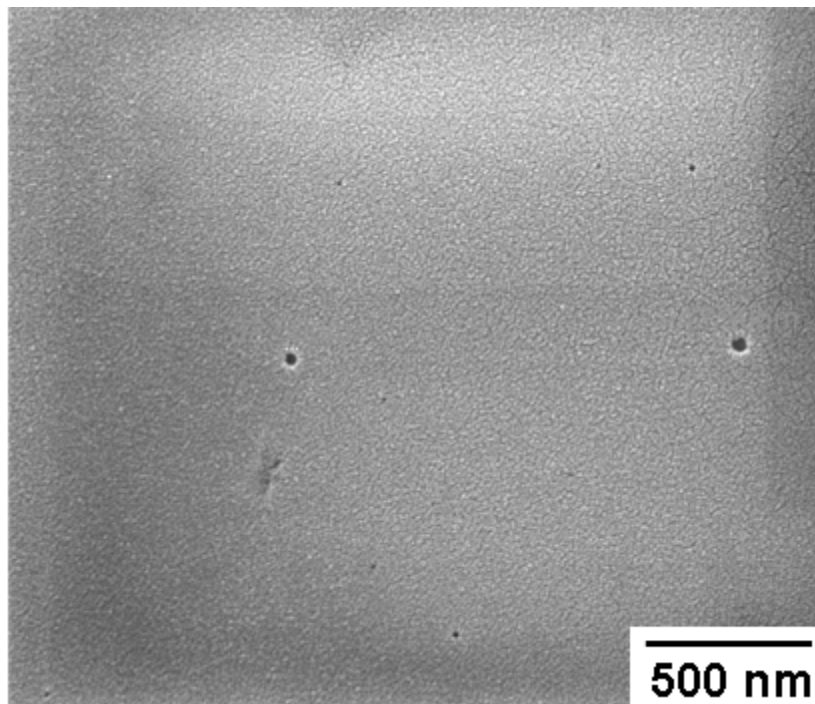


Figure 4. 24 PS M_w : 5,000 g/mole, solvent was Ethanol/THF

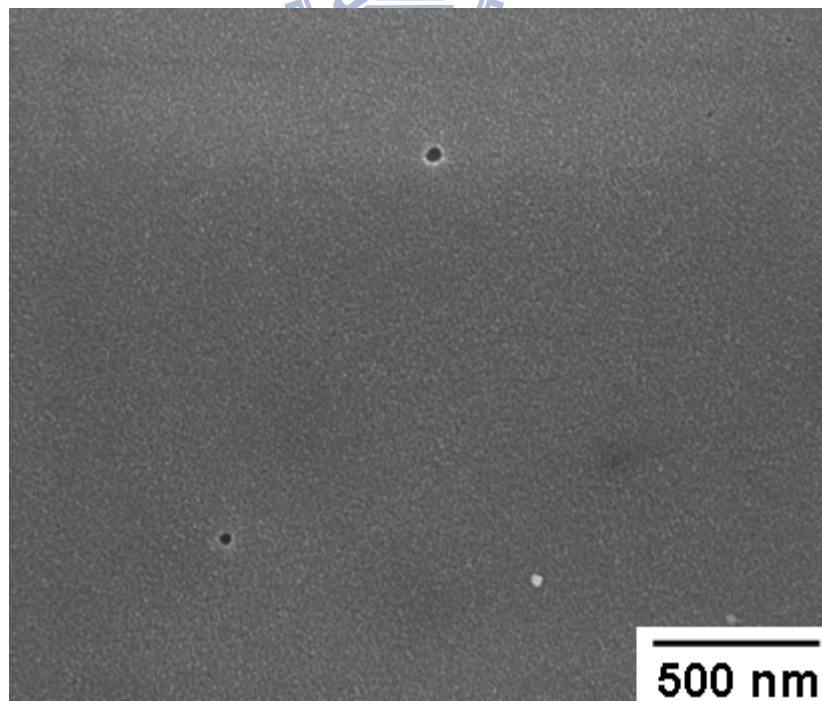


Figure 4. 25 PS M_w : 5,000 g/mole, solvent was n-Hexane/THF

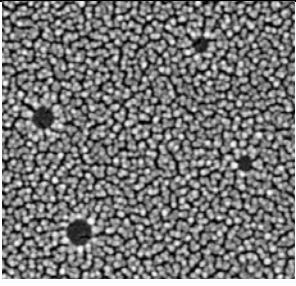
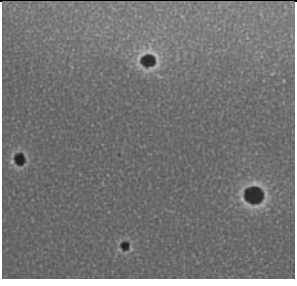
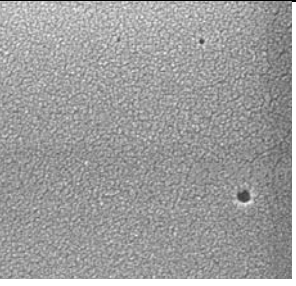
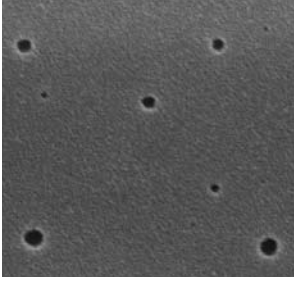
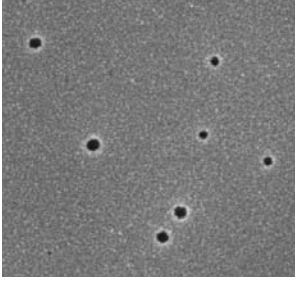
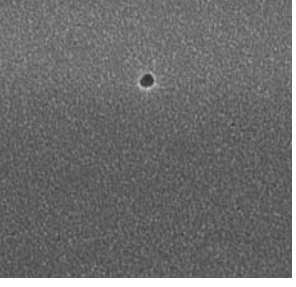
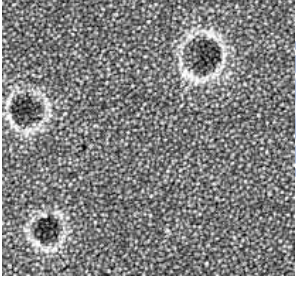
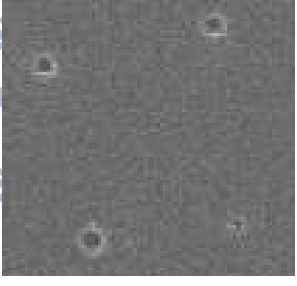
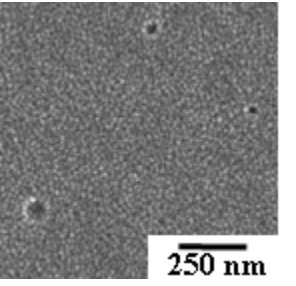
	M_w : 80,000 g/mole	M_w : 10,000 g/mole	M_w : 5,000 g/mole
Ethanol/ THF			
Pore size	80 nm	55 nm	45 nm
n-Hexane / THF			
Pore size	60 nm	45 nm	42 nm
THF			
Pore size	160 nm	100 nm	80 nm

Figure 4. 26 Summary of pore morphology and pore size

The measured pore sizes vs. the square root of PS molecular weight from various co-solvent were shown in Figure 4.27 (a)~(c). Figure 4.27 (a): PS-Siloxane dissolved in THF, (b): PS-Siloxane dissolved in Hexane /THF co-solvent, and (c): PS-Siloxane dissolved in Ethanol/THF co-solvent. When PS-Siloxane was dissolved in THF, pore size was affected by PS molecular weight. However, PS molecular weight did not

affect pore size obviously when PS was dissolved in ethanol/THF co-solvent or hexane/THF co-solvent. These three curves were fitted with Equation 4.3 ($R=a(M)^b$), where a represented diffusion parameter and b represented polymer viscosity as summarized in Table 4.3. When polymer has higher solubility in the solvent, polymer viscosity was higher. From Table 4.3, PS-Siloxane has highest viscosity in THF, thus, PS-Siloxane was well dissolved in THF.

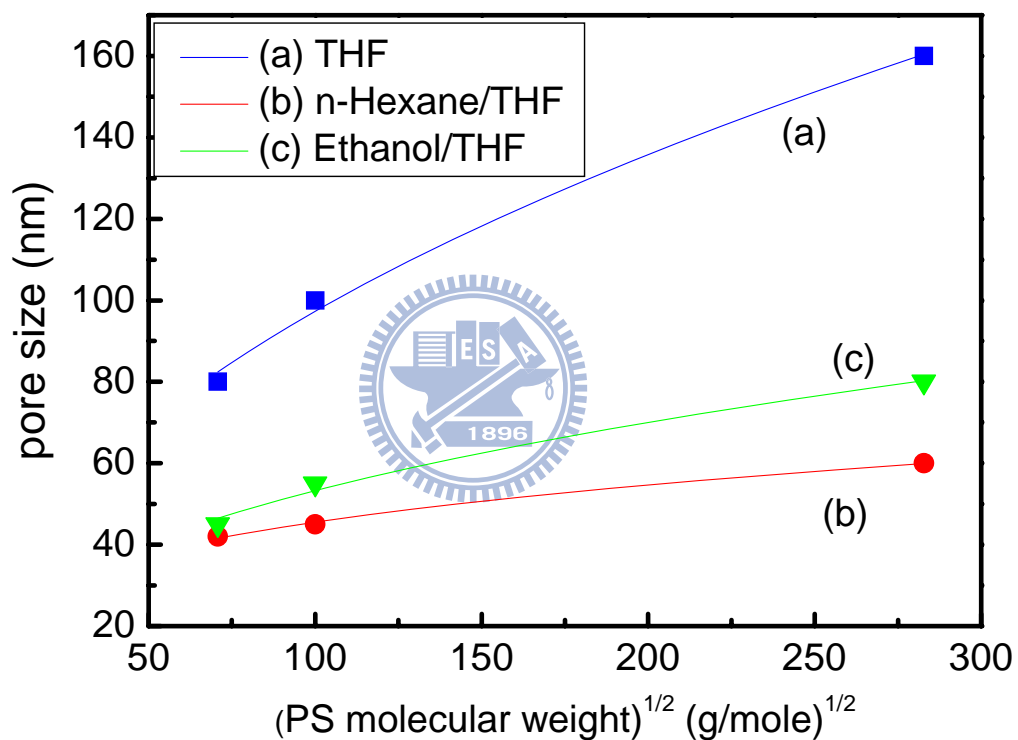


Figure 4. 27 Solvent effect of pore size

Table 4. 3 Parameters of $R=a(M)^b$ for various solvents

	a	b
THF	10.64	0.24
Ethanol/THF	13.52	0.19
Hexane/THF	8.66	0.13

Due to the solubility was the important factor of pore size, the mechanism of polymer dissolved in the solvent was illustrated in Figure 4.28. Equation 4.4 shows Gibbs free energy model for mixing of liquids, where δ was solubility parameter of solvent. Dissolution can occur spontaneous when δ_1 equal to δ_2 , and dissolution occurred when δ_1 and δ_2 were totally different. The solubility parameter of solvent closed to PS-Siloxane was good solvent, and the solubility parameter of solvent has long distance to PS-Siloxane was poor solvent. Table 4.4 shows the solubility parameters of various solvents [75] and PS [76]. From Table 4.4, ethanol and hexane were poor solvent for PS-Siloxane, but THF was good solvent. Figure 4.26 shows the mechanism of PS-Siloxane in good/ poor solvent. When PS-Siloxane was dissolved in THF, the long chain of PS was extended. Nevertheless, when PS-Siloxane was dissolved in ethanol/THF co-solvent or hexane/THF co-solvent, the long chain of PS was retracted. When PS long chain is extended in good solvent, it yields large pore. But, retracted PS long chain would result in small pore.

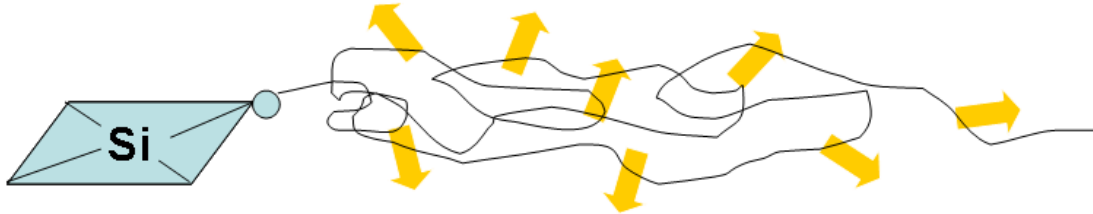
$$\Delta H_m \propto (\delta_1 - \delta_2)^2 \quad (4.4)$$

Table 4. 4 Solubility parameters for various solvents

	Ethanol	n-Hexane	THF	Polystyrene
Solubility parameter [(MPa) ^{1/2}]	26.0	14.9	18.6	16.6-20.2

Good Solvent - THF

$$\delta_{\text{THF}}(18.6) \sim \delta_{\text{PS}}(16.6-20.2)$$



Good Solvent + Poor Solvent

$$\delta_{\text{THF}}(18.6) \sim \delta_{\text{PS}}(16.6-20.2)$$
$$\delta_{\text{EtOH}}(26) > \delta_{\text{PS}}(16.6-20.2)$$

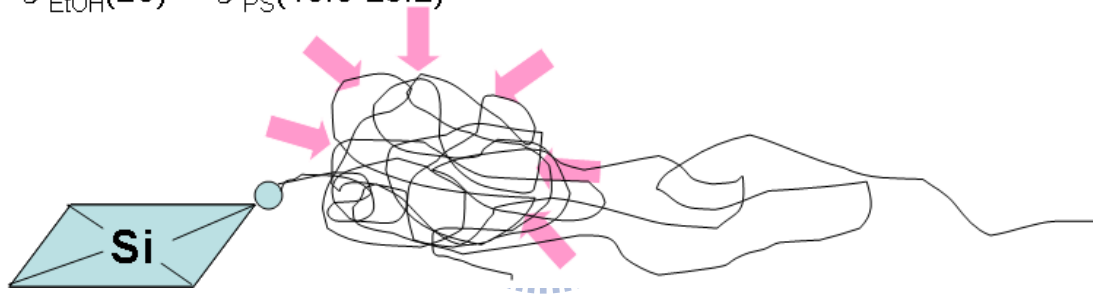


Figure 4. 28 The mechanism of PS activity in good solvent or in poor solvent

4.4.3 Porosity

Porosity of MSQ-g-PS low k film was measured and calculated by XRR. In this study, the angle of XRR scanning was from 0° to 2.5° . The scanning proceeded at very low angle, and would obtain total reflection. The angle of first drop occurred was named critical angle which was related to the electron density of the thin film. Equation 4.5 shows the relationship between critical angle and thin film density, where θ_{crit} represented critical angle and δ represented thin film density.

$$\theta_{crit} = (2\delta)^{1/2} \quad (4.5)$$

When the density of thin film has known, The film porosity could be calculated by the Equation 4.6, where ρ is film density (g/cm^3), ρ_s is MSQ density, and P refers to porosity [77].

$$\rho = \rho_s(1 - p) \quad (4.6)$$

The calculations of MSQ-g-PS porous low k film density and porosity were obtained and summarized in Table 4.4. The decreased with increasing PS molecular weight. In the same PS content, numbers of PS-Siloxane increased when PS molecular weight decreased. More PS-Siloxane unit caused more pore, thus, increased porosity.

Table 4. 5 Calculation of density and porosity

	MSQ-g-PS PS MW: 80,000	MSQ-g-PS PS MW: 10,000	MSQ-g-PS PS MW: 5,000	MSQ
Density (g/cm^3)	2.254	2.113	2.055	2.550
Porosity (%)	11.6	17.1	19.4	

4.5 Comparison between MSO-g-PS and MSQ/PS hybrid porous low k films

In order to compare the difference between MSO-g-PS porous low k film and MSQ/PS hybrid porous low k film. The MSQ/PS hybrid porous low k film was formed by mixing PS into MSQ. Figure 4.29 shows the morphology of MSQ/PS hybrid porous low k film. PS would aggregate in the solution or in thermal processing step, thus, the pore size distribution of MSQ/PS hybrid porous low k film may be wide. There were pore aggregation in MSQ/PS hybrid porous low k film, and the pore size distribution was seen as from 165 nm to 275 nm. The precise pore size/distribution should be measured by GISAXS in the future. Figure 4.30 illustrated the SEM photograph of MSQ/PS hybrid porous low k film vs. MSQ-g-PS porous low k film. PS of PS/MSQ hybrid film did not have siloxane functional group to combine with MSQ, thus, PS was free in the MSQ solution. Moreover, the solubility parameter of PS and MSQ were different, PS has more chance to aggregate in the solvent or in heating process. Furthermore, PS of MSQ-g-PS porous low k film was stock in MSQ structure, and hard to aggregate with another PS portion. Therefore, aggregation of MSQ-g-PS porous low k film was fewer than MSQ/PS hybrid porous low k film, and MSQ-g-PS improved the issue of aggregation.

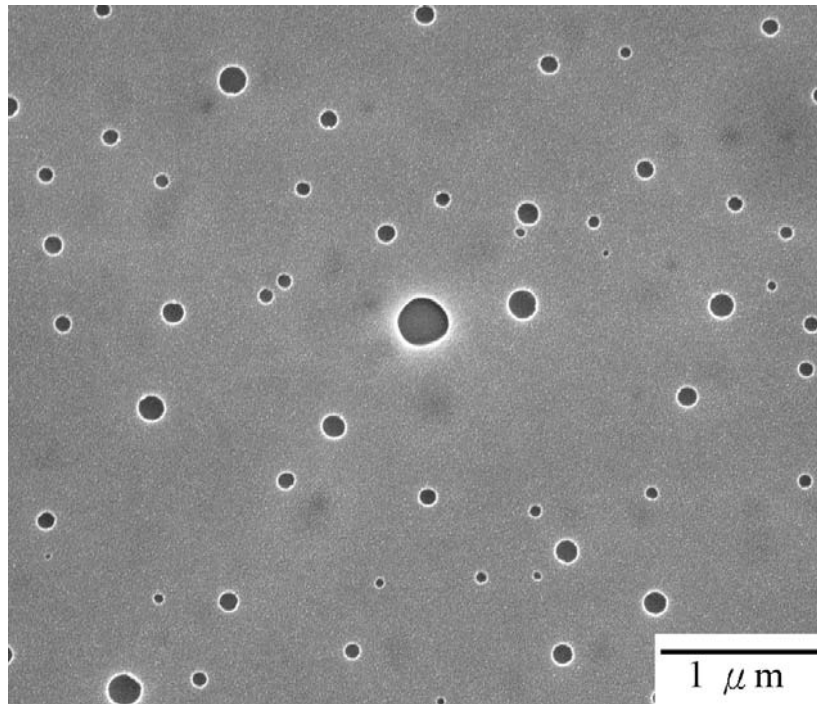


Figure 4. 29 Morphology of MSQ/PS hybrid porous low k film

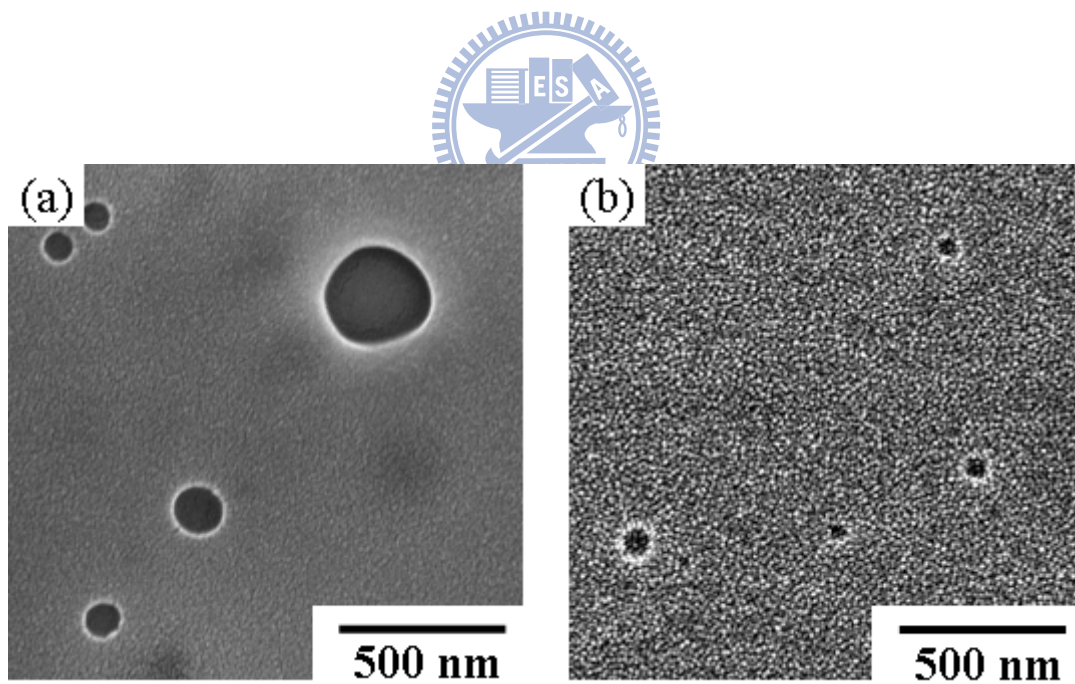


Figure 4. 30 Morphology of (a)MSQ/PS hybrid porous low k film (PS M_w :90,000 g/mole) and (b) MSQ-g-PS porous low k film (PS M_w :80,000 g/mole)

Chapter 5 Conclusion

In order to overcome the issues of Solid-FirstTM faced, a novel method was invented to improve these problems. Grafting material was proposed to replace the commercial hybrid material on porous low k film. Grafting material: PS-Siloxane has end-capped siloxane and high decomposition temperature can be used as high-temperature porogen in this study. MSQ-g-PS was synthesized by grafting PS-Siloxane onto MSQ through siloxane group. This thesis focus on major topics: (1) synthesis of siloxane end-capped PS, and the grafting of PS-Siloxane onto MSQ through siloxane group, (2) the relationship between PS molecular weight and pore size, (3) solvent effect on pore size, and (4) the pore morphology between MSQ-g-PS and PS/MSQ hybrid porous low k films.

PS with siloxane end-cap was synthesized by ATRP, its molecular weight can be controlled by the content of initiator. Using ATRP can obtain polymer which has low polydispersity index. PS-Siloxane grafted onto MSQ through siloxane group by sol-gel method. The novel compound was named “MSQ-g-PS” which structure was investigated by TGA, FTIR, and ²⁹Si-NMR.

Pore size decreased from 160 nm to 90 nm when PS molecular weight decreased from 80,000 g/mole to 5,000 g/mole. PS molecular weight was the direct factor of pore size. However, synthesis of low molecular weight PS faced bottlenecks: (1) PDI was uncontrollable, and (2) radical could die in the process. Finding a new and simple way to decrease pore size is imperious, thus, solvent effect was proposed. The difference solubility parameter between solvent and PS would change the status of PS long chain. PS long chain was retracted in poor solvent. Therefore, using co-solvent (EtOH/THF, Hexane/THF) can retract PS long chain and decrease pore size.

PS/MSQ hybrid film was obtained to compare to MSQ-g-PS film. Pore size of MSQ-g-PS porous low k film (PS $M_w = 80,000$ g/mole) were 160 nm, but pore size of PS/MSQ hybrid film (PS $M_w = 90,000$ g/mole) were from 165 to 275 nm. PS would aggregate on PS/MSQ hybrid film, and caused poor pore size distribution. MSQ-g-PS film would not have pore aggregation, because of the steric hindrance of MSQ would separate porogen, thus, MSQ-g-PS was a novel and great material for using on ILD.

MSQ-g-PS is a novel material, which can avoid pore aggregation and control pore size. MSQ-g-PS improved the issues of Solid-First™ faced and opened a new sight of ILD layer material.



References

- [1] M. T. Bohr, and Y. El-Mansy, Proc. Of 1988 Symp. On VLSI Technology”, 95 (1988)
- [2] International Technology Roadmap for Semiconductors, Executive Summary (2005)
- [3] Y. H. Wang and R. Kumar, J. Electrochem. Soc., **151**, 73 (2004)
- [4] X. Y. Bao, X. S. Zhao, X. Li, and J. Li, Applied Surface Science, **237**, 380, (2004)
- [5] S. Malhouitre, C. Jehoul, J. V. Aelst, H. Struyf, S. Brongersma, L. Carbonell, I. Vos, G. Beyer, M. V. Hove, D. Gronbeck, M. Gallagher, J. Calvert and K. Maex, Micro. Eng. **70**, 302 (2003)
- [6] M. L. Che et. al., 2008 IEDMS: oral section AO-424 (2008)
- [7] H.J. Lee, C.L. Soles, B.D. Voqt, D.W. Liu, W.L. Wu, E.K. Lin, H.C. Kim, V.Y. Lee, W. Volksen, and R.D. Miller, Chemistry of Materials, **20**, 7390 (2008)
- [8] A. Zenasni, F. Ciaramella, V. Jousseume, Ch. Le Cornec, and G. Passemard, Journal of The Electrochemical Society, **154** (1), G6-G12 (2007)
- [9] J. Kovacik, Journal of Materials Science Letters, **18**, 1007 (1999)
- [10] X. Yao, L. Zhang, and S. Wang, Sensors and Actuators B, **24**, 347 (1995)
- [11] Y. H. Chen et al, 2008 MRS Fall Meeting, 510449 (2008)
- [12] International Technology Roadmap for Semiconductor, Executive summary, 2005
- [13] S. J. Martin, J. P. Godschalx, M. E. Mills, E. O. Shaffer II, and P. H. Townsend, Advanced Materials, **12**, 1769 (2000)
- [14] R. J Gutmann, IEEE Trans. Microw. Theory Tech. **47**, 667 (1999)
- [15] M. Bohr: Tech. Digest IEEE Int. Electronic Device Meeting, 241 (1995)
- [16] D. C. Edelstein, J. Heidenreich, R. Goldblatt, W. Cote, C. Uzoh, N. Lustig, P. Roper, T. McDevitt, W. Motsiff, A. Simon, J. Dukovic, R. Wachnik, H. Rathore, R. Schulz, L. Su, S. Luce, J. Slattery: in IEEE Int. Electron Device Meeting, **773** (1997)
- [17] D. C. Edelstein, G.A. Sai-Halasz, Y. J. Mii: IBM J. Res. Dev., **39**, 383 (1995)
- [18] T. C. Chang, P. T. Liu, Y. J. Mei, Y. S. Mor, T. H. Perng, Y. L. Yang and S. M. Sze, J. Vac. Sci. & Technol. B, **17**, 2325 (1999)
- [19] K. Yonekura, S. Sakamori, K. Goto, M. Matsuura, N. Fujiwara and M. Yoneda, J.

-
- Vac. Sci. Technol. B, **22**, 548 (2004)
- [20] A. Matsushita, N. Ohashi, K. Inukai, H. J. Shin, S. Sone, K. Sudou, K. Misawa, I. Matsumoto and N. Kobayashi, Proc. Int. Interconnect Technol. Conf., San Francisco, 147 (2003)
- [21] K. Mosig, T. Jacobs, K. Brennan, M. Rasco, J. Wolf, and R. Augur, Microelectronic Engineering, **64**, 11 (2002)
- [22] M. Ree, K. J. Chen, D. P. Kirby, J. Appl. Phys., **72**, 2014 (1992)
- [23] G. Hougham, G. Tesoro, A. Viehbeck, J. D. Chapple-Sokol, Macromolecules, **27**, 5964 (1994)
- [24] D. I. Bower, An Introduction to Polymer Physics, Cambridge University, Chapter 9 (2002)
- [25] G. Huougham, G. Tesoro, A. Viehbeck and J. D. Chapple-Sokol, Macromolecules, **27**, 5964 (1994)
- [26] C. H. Ting, T.E. Seidel, Materials Research Society Symposium - Proceedings, Low-Dielectric Thin Films for Micoelectronics Applications, 124 (1995)
- [27] H. H. Huang, B. Orier, and G. L. Wilkes, Polym. Bull., **14**, 557 (1985)
- [28] S. Loo, S. Idapalapati, S. Wang, L. Shen and S. G. Mhaisalkar, Scripat Materials, 57, 1157 (2007)
- [29] I. Sugiura, N. Misawa, S. Otsuka, N. Nishikawa, Y. Iba , F. Sugimoto, Y. Setta, H. Sakai, Y. Koura, K. Nakano, T. Karasawa, Y. Ohkura, T. Kouno, H. Watatani, Y. Nakata, Y. Mizushima, T. Suzuki, H. Kitada, N. Shimizu, S. Nakai, M. Nakaishi, S. Fukuyama, T. Nakamura , E. Yano, M. Miyajima, and K. Watanabe, Microelectronic Engineering, 82, 380 (2005)
- [30] C. J. Brinker, Y. Lu, A. Sellinger, H. Fan, Adv. Mater, **11**, 579 (1999)
- [31] P. S. Ho, J. Leu, and W. W. Lee, Low Dielectric Constant Materials for IC Applications , Chapter 6 (2002)
- [32] A. Sayari, I. Moudrakovski, J. S reddy, C. I. Ratcliffe, J. A. Pipmeester and K. F. Preston, Chem. Mat, **8**, 2080 (1996)
- [33] J. M. Thomas, O. Terasaki, P. L. Gai, W. Zhou and J. Gonzalez-Calbe, Accounts. Chem. Res., **34**, 583 (2001)
- [34] Y. H. Sakamoto, M, Kaneda, o. Terasaki, D. Y. Zhou, J. M. Kim, G. Stucky, J. Shin and R. Ryoo, Nature, **408**, 449 (2000)
- [35] M. Kruk, M. Jaroniec, Y. Sakamoto, O. Terasaki, R. Ryoo and C. H. Ko, J. Phys.

-
- Chem. B, **104**, 292 (2000)
- [36] Q. Huo, D. I. Margolese, U. Ciesla, P. Feng, T. E. Gier, and G. D. Stucky, *Nature*, **368**, 317 (1994)
- [37] P. T. Tanev and T. J. Pinnavaia, *Science*, **267**, 865 (1995)
- [38] D. Y. Zhao, J. L. Feng, Q. S. Huo, N. Melosh, G. H. Fredrickson, B. F. Chmelka and G. D. Stucky, *Science*, **279**, 548 (1998)
- [39] M. S. Wong and J. Y. Ying, *Chem. Mat.*, **10**, 2067 (1998)
- [40] K. Mosig, T. Jacobs, K. Brennan, M. Rasco, J. Wolf and R. Augur, *Micro. Eng.*, **64**, 11(2002)
- [41] C. M. Stafford, C. Harrison, K. L. Beers, A. Karim, E. J. Amis, M. R. Vanlandingham, H. C. Kim, W. Volksen, R. D. Miller, and E. E. Simonyi, *nature materials*, **3**, 545 (2004)
- [42] C. M., Wittkowski, T., Jung, K., Hillebrands, B. and Baklanov, M. R *Appl. Phys. Lett.*, **80**, 4594 (2002).
- [43] E. Huang, *Appl. Phys. Lett.*, **81**, 2232 (2002).
- [44] J. A. Hedstrom, *Langmuir*, **20**, 1535 (2004)
- [45] K. K. Phani, and S. K. Niyogi, *J. Mater. Sci.*, **22**, 257 (1987)
- [46] T. Abell and K. Maex, *Micro. Eng.*, **76**, 16 (2004)
- [47] T. Otsu, M. Yoshida, and T. Tazaki, *Makromol. Chem. Rapid. Commun.*, **3**, 133 (1982)
- [48] J. F. Lutz, and K. Matyjaszewski, *Macromol. Chem. Phys.*, **203**, 1385 (2002)
- [49] K. Matyjaszewski, and J. Xia, *Chem. Rev.*, **101**, 2921 (2001)
- [50] K. A. David, and K. Matyjaszewski, *Macromolecules*, **34**, 2101 (2001)
- [51] M. K. Georges, R. P. N. Veregin, P. M. Kazmaier, and G. K. Hamer, *Macromolecules*, **26**, 2987 (1993)
- [52] F. D'Agosto, R. Hugher, M. T. Charreyre, C. Pichot, and R. G. Gilbert, *Macromolecules*, **36**, 621 (2003)
- [53] J. F. Rabek, *Experimental Methods in Polymer Chemistry*, Wiley-Interscience, New York, Chap. 25, (1980)
- [54] K. H. Altgelt and L. E. Segal, *Gel Permeation Chromatography*, Marcel Dekker, New York, Chap. 20 (1971)

-
- [55] L. H. Tung, M.I Dekker, N. York, L. H. Tung and J. C. Mppre., Fractionation of Synthetic Polymers Chap.6. (1977)
- [56] R. P. Scott and P. Kucera, J. Chromatogr. Sci., **9**, 641 (1971)
- [57] D. Noble, Anal. Chem., **67**, 323 (1995)
- [58] R.F. Schwenker and P. D. Garm, New York: Academic Press, 1, 68 (1969)
- [59] C. M. Earnest, Anal. Chem., **56**, 1471 (1984)
- [60] K. Dovstam, Int. J. Solid Structure, **32**, 2835 (1995)
- [61] C. A. Lucas, P. D. Hatton, S. Bates, W. Ryan, S. Miles, and B. K. Tanner, J Appl. Phys., **63**, 1936 (1988)
- [62] S. G. Weissberg, S. Rothman, and M. Wales, Analytical Chemistry of Polymer, Part2, Chap1 (1962)
- [63] H. D. H. Stover and J. M. J. Frbchet, Macromolecules, **24**,883 (1991)
- [64] S.Andras and P.Alfredo, J. Phys. Chem. A., **109**, 8385 (2005)
- [65] P. W. Fowler, A. Rogowska, A. Soncini, M. Lillington, and L. P. Olson, J. Org. Chem., **71**, 6459 (2006)
- [66] H. Fischer, J. polym. Sci. Chem. Ed., **37**, 1885 (1999)
- [67] D. A. Shipp and K. Matyjaszewski, Macromolecules, **32**, 2984 (1999)
- [68] G. Odian, Princples of Polymerization Fourth edition, Chap 1, 23 (2004)
- [69] T. Iwasaki and J. I. Yoshida, Macromolecules, **38**, 1159 (2005)
- [70] A. Grill, and D. A. Neunayer, J. Appl. Phys., 94, 6697 (2003)
- [71] T. Abellm K. Houthoofd, F. Iacopi, P. Grobet, and K. Maex, Mat. Res. Soc. Sympm Proc., 863, B1.8.1 (2005)
- [72] M. Netopilok, and P. Kratochvil, Polymer, **44**, 3431 (2003)
- [73] K. Terao and J. M. Mays, European Polymer Journal, **40**, 1623 (2004)
- [74] M.P. Vega, E.L. Lima, and J.C. Pinto, Polymer, **42**, 3909 (2001)
- [75] J.Brandrup, Polymer Handbook, VII/526, 3rd, John Wiley & Sons, New York (1989)
- [76] J. Brandrup, Polymer Handbook, V/81, 3rd, John Wiley & Sons, New York (1989)
- [77] W. Wu, J. Appl. Phys., **87**, 1193 (2000)